

Transport properties in non-Fermi liquid phases of nodal-point semimetals

Ipsita Mandal^{1,2} and Hermann Freire³

¹*Department of Physics, Shiv Nadar Institution of Eminence (SNIOE),
Gautam Buddha Nagar, Uttar Pradesh 201314, India*

²*Freiburg Institute for Advanced Studies (FRIAS),
University of Freiburg, D-79104 Freiburg, Germany*

³*Instituto de Física, Universidade Federal de Goiás, 74.001-970, Goiânia-GO, Brazil*

In this review, we survey the current progress in computing transport properties in semimetals which harbour non-Fermi liquid phases. We first discuss the widely used Kubo formalism, which can be applied to the effective theory describing the stable non-Fermi liquid phase obtained via a renormalization group procedure and, hence, is applicable for temperatures close to zero (e.g., optical conductivity). For finite temperature regimes, which apply to the computations of the generalized dc conductivity tensors, we elucidate the memory matrix approach. This approach is based on an effective hydrodynamic description of the system, and is especially suited for tackling transport calculations in strongly-interacting quantum field theories, because it does not rely on the existence of long-lived quasiparticles. As a concrete example, we apply these two approaches to find the response of the so-called *Luttinger-Abrikosov-Benelavskii phase* of isotropic three-dimensional Luttinger semimetals, which arise under the effects of long-ranged (unscreened) Coulomb interactions, with the chemical potential fine-tuned to cut exactly the nodal point. In particular, we focus on the electric conductivity tensors, thermal and thermoelectric response, Raman response, free energy, entropy density, and shear viscosity.

CONTENTS

I. Introduction	1
II. Transport methodologies beyond the Fermi liquid paradigm	3
A. Kubo formula	4
1. Expectation value in the linear response regime	4
2. The Kubo identity and the retarded Green's function in the frequency domain	5
3. Conductivity tensor	6
B. Memory matrix formalism	7
1. Memory function formalism	7
2. Generalized conductivity tensors in the absence of magnetic fields	9
3. Generalized conductivity tensors in the presence of a weak magnetic field	11
C. Generic scaling arguments	11
III. Transport properties of the LAB phase	12
A. Minimal low-energy effective model	12
B. Optical electrical conductivity	14
C. dc electrical conductivity	14
D. Thermal and thermoelectric response	15
E. Raman response	15
F. Shear viscosity and entropy density	17
IV. Discussion and Outlook	18
Acknowledgments	19
References	19

I. INTRODUCTION

The Landau's Fermi liquid theory has been incredibly successful in describing most metallic phases, serving as a

paradigm to treat condensed matter systems in terms of quasiparticles and their effective interactions. However, we are aware of metallic states with unconventional/strange properties for which the paradigmatic description in terms of Fermi liquids fails. Although of widely different origins, these systems are widely known as non-Fermi liquids (NFLs), in which the quasiparticles get destroyed, often brought about by the strong interactions of the soft fluctuations at a Fermi surface/Fermi point with some massless bosonic fluctuations. There has been intensive efforts in formulating controlled approximations to describe such NFL phases involving a well-defined Fermi surface [1–24]. Such metallic states are often dubbed as *strange metals* because of the observation of strange transport properties in many strongly-correlated quantum materials such as cuprate superconductors [25–27], iron-based superconducting compounds [28], some heavy fermion materials [29], and magic-angle twisted bilayer graphene [30, 31]. Instead of a conventional quadratic dependence on the temperature T , the normal phases of these materials/heterostructures often show a linear-in- T resistivity within a large temperature window, violating the Mott-Ioffe-Regel limit. Other manifestations of an NFL behaviour involve novel scaling-dependence of optical conductivity [17, 19, 32, 33] and enhanced susceptibility towards superconducting instability [8, 9, 18, 19, 34]. In these scenarios, which involve a finite and sharply defined Fermi surface (although no Landau quasiparticles), the NFL character emerges due to finite-density fermions interacting with a massless boson arising at a quantum critical point [6, 7, 11, 13, 14, 21, 31], or with massless gauge field(s) [8, 9, 22, 35], leading to the alternate name of *critical Fermi surface states* [36]. However, additionally, there has been the investigation of NFL phases appearing at a Fermi point, i.e., when the chemical potential cuts a band-crossing point in a semimetal [37–44], which is the focus of this review article. For these cases, when the Fermi level tuned at the band-touching points of semimetals in the presence of long-ranged Coulomb inter-

actions [37–39, 43, 44], a stable non-Fermi liquid fixed point emerges.

Transport coefficients, such as the electrical and thermal conductivity and the viscosity tensors, play a central role in describing condensed matter systems. They are experimentally measurable and contain signatures which characterize the different phases of matter. Computing such transport properties using the effective theories of NFLs states is challenging, because we cannot use the conventional frameworks available, as described below. Determining transport properties implies that we want to theoretically compute the response of the system to an external perturbation. If the perturbation is small, the response is expected to be a linear function of the perturbation. This is the basic assumption of *linear response theory*. In the framework of many-particle theory, the linear response theory results in the Kubo formula (detailed discussion can be found in Sec. II A), which refers to relations that express the linear response function in terms of the equilibrium eigenstates of the system, and were first obtained by Kubo [45, 46]. However, let us first discuss a different route, mainly to explain why it does not work for the NFL systems we want to analyze. If the external perturbation changes slowly in time and space on atomic scales, we can use a semiclassical description known as the Boltzmann formalism. This formalism originates from the Boltzmann equation (BE), introduced by Boltzmann in 1872, to study irreversibility in dilute (i.e., low-density) gases from a statistical mechanics point of view. He obtained the BE by visualizing the dynamics of the constituent gas-molecules as free motions, occasionally interrupted by mutual collisions. In the modern literature, the term BE is used in a very wide context (or a more generic sense), referring to any kinetic equation that describes the change of a macroscopic quantity (such as density of energy, charge, or particle number) in a thermodynamic system. In particular, the transport properties in a condensed matter systems are often related to the well-defined quasiparticle-excitations, which, at a phenomenological level, resemble a dilute gas of molecules for which a BE (or a closely related kinetic equation) can indeed be formulated. The quasiparticle concept is crucial to applying the Boltzmann transport concept in condensed matter. Depending on the physical system under consideration, various types of quasiparticles emerge quantum-mechanically (for example, dressed electrons in metals), whose kinetics can then be modelled by an appropriate semiclassical approach of the BE. The idea is to consider the phase space distribution function $f(\mathbf{r}, \mathbf{k}, t)$ of the quasiparticles, and determine the evolution of $f(\mathbf{r}, \mathbf{k}, t)$ in phase space by using the Liouville equation (arising from the Liouville theorem) modified by adding the correction term arising due to quasiparticle-collisions as a perturbation [47]. However, the bootmline is, since the BE crucially depends on the existence of well-defined and long-lived fermionic quasiparticles, the absence of quasiparticles in NFLs is a major impediment to using it for NFLs. Nevertheless, we must add that the methodology of invoking a generalized quasiparticle distribution, within the nonequilibrium Keldysh formalism, has been employed in extracting the behaviour of collective modes of critical Fermi surfaces [48–51].

Another limitation of BE approach stems from the fact

that we use a semiclassical distribution function for computing the transport properties. The Kubo formalism [45, 46] remedies this issue by replacing the semiclassical statistics with quantum statistics. The move from classical statistical mechanics to quantum statistical mechanics is implemented by calculating the average of a macroscopic observable by its trace weighted with the density matrix of the system. Kubo’s linear response formalism, we compute the linear-order response coefficient as a correlation function of the operator of interest and the operator which couples to the applied external probe field. In fact, the Kubo formula gives the exact linear-order response function, as no approximations are made in its derivation. Therefore, it captures the quantum coherent effects that cannot be captured by Boltzmann transport theory. On the other, since the time evolution in the Kubo formula is evaluated by tracking the full microscopic dynamics through the time evolution operator constructed out of the equilibrium Hamiltonian of the system. Therefore, it can work only if we have a controlled perturbative description of the corresponding quantum field theory, where the free part of the quantum effective action can be used to find the exact eigenstates and energies of the system, which feed into the expressions for the correlation functions. For NFLs, we can thus use the Kubo formula only if we succeed in achieving a controlled perturbative expansion and, using the theory in the vicinity of a stable NFL fixed point, we can then compute the required correlators using the order-by-order perturbative corrections.

We have now understood that although the Kubo formalism is an improvement upon the Boltzmann transport theory by replacing classical statistical mechanics with quantum statistical mechanics, it does not include the coarse-graining of the microscopic dynamics which renders the Boltzmann transport theory tractable in the thermodynamic limit. The memory matrix formalism [52–59] addresses this problem by devising a method of coarse-graining that is compatible with quantum statistical mechanics. Because the Kubo formalism is an exact quantum statistical mechanical description, it is a very useful starting point. Hence, the memory matrix approach is not so much different, as it is a reformulation of the time evolution in the Kubo formalism by making the coarse-graining approximations natural. The general philosophy of a coarse-graining procedure is to (1) find the most relevant collective variables to describe a macroscopic system, (2) separate out the contributions arising from the relevant variables and rewrite the equations of motion for the relevant variables, and (3) approximate the effects of the irrelevant variables on the evolution of the relevant operators. This leads to a macroscopic equation of motion, governing the evolution of the relevant observables, that reproduces the most interesting and leading order manifestation of the underlying microscopic physics. A simple example is obtained from the Navier–Stokes equation in hydrodynamics, which describes the motion of viscous fluids in terms of the collective variables of pressure, density, and flow, rather than by tracking the positions and velocities of individual molecules. Such a description is derived from the microscopic physics by applying universal constraints like conservation of particle number and conservation of momentum, which brings into

consideration the behaviour of the average density and the average flow, ignoring the microscopic fluctuations. In a similar spirit, the memory matrix procedure starts with applying the Mori projection on the equations of motion for the operators, obtained using the same time evolution as used in the Kubo formalism. After splitting the dynamics into the subspaces of the relevant and irrelevant operators, the so-called Mori's projected equations of motion consist of the generalized Langevin equations for the relevant dynamical variables, with the effects of the irrelevant operators appearing in the equations as correlation functions with the relevant operators. In recent times, this formalism has attracted a significant amount of interest, especially because it has successfully reproduced the signature transport properties of many strongly-coupled systems, which were earlier computed from nonperturbative approaches (e.g., those obtained by exploiting the gauge-gravity duality between the strongly-coupled quantum field theory and the corresponding classical gravity theory in one higher spatial dimension [60, 61]).

In view of the discussed presented above, both the Kubo formula and the memory matrix formalism have emerged as central tools to compute the transport coefficients of various NFL phases exhibited by correlated quantum materials. In this review, we will demonstrate how these two approaches can be employed to compute the scalings of various response coefficients of a nodal-point NFL.

In recent years, modelling and understanding NFL behaviour has witnessed enormous progress in connection with the various aspects of the transport properties of strange-metallic-phases. Such descriptions include strongly-correlated systems like the Sachdev-Ye-Kitaev (SYK) models [24, 62–69], strongly-coupled field theories that are holographically dual to black hole physics [60, 61, 70–72], and experimentally-motivated phenomenological models describing high- T_c materials [17, 19, 33, 73–83]. However, these systems involve a finite Fermi surface, while we will mostly be interested in NFL phases appearing at Fermi points. Important examples of nodal-point NFLs are described below:

1. From the analysis of the electronic bandstructures of compounds like pyrochlore iridates [84], half-Heusler compounds [85, 86], grey-tin [87], and rhodium oxides [88], a minimal effective low-energy model to describe such systems turns out to be the well-known three-dimensional (3d) Luttinger semimetals [37–42, 89–93]. The resulting dispersion has a single doubly-degenerate quadratic band crossing at the center of the Brillouin zone (i.e., at the Γ -point). This novel class of materials feature a strong spin-orbit coupling (SOC) and, together with a strong electron-electron interaction caused by unscreened Coulomb interactions, demonstrate Mott correlation physics and NFL behaviour. The itinerant NFL physics was predicted theoretically back in 1974 by Abrikosov [37], who demonstrated, using the quantum field theoretical framework, that the Coulomb interactions drive the system into a stable NFL fixed point, which is now widely known as the *Luttinger-Abrikosov-Beneslavskii (LAB) phase* [39]. Moon *et al.* [39] revisited this problem and characterized the NFL

fixed point using a dimensional regularization scheme, which enabled them to calculate the universal power-law exponents describing various physical observables like conductivity, susceptibility, specific heat, and the magnetic Gruneisen number. The data from experiments [84] on the pyrochlore iridate $\text{Pr}_2\text{Ir}_2\text{O}_7$ show evidence for the LAB phase.

2. Quasiparticles with pseudospin-3/2 and having a birefringent linear spectrum with two distinct Fermi velocities, can be realized from simple tight-binding models in both two-dimensional (2d) and three-dimensional (3d) systems. Examples in 2d include decorated π -flux square lattice [94–96], honeycomb lattices [97, 98], and shaken optical lattices [99, 100]. The 3d counterparts are captured in various systems having strong spin-orbit coupling [101, 102], such as the antiperovskite family [103] (with the chemical formula A_3BX) and the CaAgBi -family materials with a stuffed Wurtzite structure [104]. The low-energy effective Hamiltonian of such semimetals show that Coulomb interactions drive a clean system (i.e. without disorder) into a marginal Fermi liquid phase [43, 44] in both 2d and 3d.

Using the dimensional regularization scheme (applied to the Kubo formula) and the memory matrix formalism, we computed various transport properties of the LAB phase, which we will summarize in this review [105–108].

The review is organized as follows. In Sec. II, we review the Kubo formalism and the memory matrix technique to set the stage for deriving the transport theories of NFL states. Sec III is devoted to the application of both the methodologies to the specific example of the LAB phase. Finally, in Sec. IV, we end with a summary and discussion, providing an outlook concerning the open problems in this field of research.

II. TRANSPORT METHODOLOGIES BEYOND THE FERMI LIQUID PARADIGM

In this section, we will discuss the basic framework of applying the Kubo formalism and the memory matrix technique to a system which can be described by a field theory action. The need for these two kinds of approaches can be motivated as follows. For NFLs at finite temperatures, there remain great difficulties in calculating transport coefficients analytically due to the lack of a quasiparticle description. This holds true even when the nature of the underlying critical point is well-understood via a controlled approximation (e.g., dimensional regularization and ϵ -expansion) and the scaling of the transport coefficients are determined by universal physics at the renormalization group (RG) flow fixed points [108]. As a simple example, let us consider the electrical conductivity σ at finite frequencies (ω) temperatures (T), which is obtained from the current-current correlation function via the Kubo formalism. Suppose the expected scaling behaviour is captured by the relation $\sigma(\omega, T) \sim T^{\frac{d-2}{z}} \mathcal{F}(\omega/T)$, where d is the dimensionality of the system in space, z is the dynamical critical exponent, and $\mathcal{F}(u)$ is a universal scaling function.

It is well-known that the small and large limits of ω and T do not commute, leading to very different physical consequences in the two regimes $\omega \gg T$ and $\omega \ll T$ [109]. The $\omega \gg T$ limit essentially corresponds to that of the $T = 0$ stable NFL fixed point of a controlled perturbative approximation of the field theory, thus enabling the current-current correlator to be computed using the $T = 0$ action. In contrast, the opposite limit of $T \gg \omega$ falls into the hydrodynamic regime of thermally activated scale-invariant excitations moving through the sample and interacting amongst themselves other over long-distance-scales. Calculating the form of the correlators in this limit is significantly more complex, even in a controlled perturbative expansion. As a result, while we can apply the Kubo formalism for computing the optical conductivity, valid in the regime $\omega \gg T$, the $T \gg \omega$ dc conductivity has to be computed by some other method, which we choose here to be the memory matrix technique.

A. Kubo formula

In this subsection, we review the Kubo formula to calculate the transport properties of a correlated model, following the treatment outlined in Refs. [110, 111]. Let the quantum system in question in its thermodynamic equilibrium state be described by the Hamiltonian $H^{(0)}$. The expectation value of a physical observable \mathcal{O} is given by

$$\langle \mathcal{O} \rangle \equiv \text{Tr}[\rho^{(0)} \mathcal{O}], \quad (1)$$

where

$$\rho^{(0)} = \frac{e^{-\beta H^{(0)}}}{\mathcal{Z}(\beta)} \quad (2)$$

is the density operator (or the density matrix), $\beta = 1/(k_B T)$ (with k_B set to unity, as we are using the natural units everywhere in this review), $\mathcal{Z}(\beta) = \text{Tr}[e^{-\beta H^{(0)}}]$ is the partition function, and T is the equilibrium temperature. We are interested in the measurement of an observable that follows some external perturbation, which helps to shed light into the inner workings of complex systems. and get dynamical information. To this end we consider the system to be coupled to an external field that is characterized by a time-dependent interaction part $V(t)$ to the Hamiltonian, leading to the total Hamiltonian

$$H^{\text{tot}}(t) = H^{(0)} + V(t), \quad (3)$$

with the new density matrix $\rho(t)$. To emphasize once more, while $H^{(0)}$ describes the quantum system in isolation, an external time-dependent $V(t)$ perturbation is applied. We will consider the scenario where the system is not affected by the perturbation in the infinite past, i.e., we are dealing with the case when $\lim_{t \rightarrow -\infty} V(t) = 0$. For example, when the external perturbation is a spatially uniform time-dependent electric field, a convenient way to realize this is via

$$\mathbf{E}(t) = \lim_{\delta \rightarrow 0^+} \mathbf{E}^{(0)} e^{-i\omega t + \delta t}, \quad (4)$$

where we have included an infinitesimal positive imaginary part to the frequency ω of a sinusoidal time-dependence. For the cases of more generic time-dependence of $V(t)$, we would use the form

$$V(t) = \lim_{\delta \rightarrow 0^+} \int_{-\infty}^{\infty} \frac{d\omega}{2\pi} \tilde{V}(\omega) e^{-i\omega t + \delta t}, \quad (5)$$

where $\tilde{V}(\omega)$ denotes the Fourier transform of $V(t)$ in the temporal space.

1. Expectation value in the linear response regime

As a consequence of the applied external perturbation, the observable \mathcal{O} becomes time-dependent as well, and its time-evolution is obtained from

$$\langle \mathcal{O} \rangle_t = \text{Tr}[\rho(t) \mathcal{O}], \quad (6)$$

where the density matrix itself obeys the von Neumann equation

$$i\hbar \partial_t \rho(t) = [H^{\text{tot}}(t), \rho(t)]. \quad (7)$$

We would like to emphasize that for $\rho(t)$ and $V(t)$, we are analyzing the time-dependence of operators that are in the Schrödinger picture, since the von Neumann equation follows for an arbitrary density matrix defined with the help of many-body wavefunctions obeying the Schrödinger equation with the Hamiltonian $H^{\text{tot}}(t)$.

Since the perturbation is switched on in the infinite past, till when the system is assumed to be in equilibrium, we have

$$\lim_{t \rightarrow -\infty} \rho(t) = \rho^{(0)}. \quad (8)$$

If we restrict ourselves to small/weak external perturbations, we can focus on the so-called *linear response regime*, which refers to retaining changes that are proportional to linear order in $V(t)$. In order to proceed further, we need to adopt the interaction picture. In this representation, the density matrix $\rho^{(I)}(t)$ [of the interaction picture Hamiltonian $H^{\text{tot}}(t)$] obeys the equation

$$\rho(t) = e^{-\frac{iH^{(0)}t}{\hbar}} \rho^{(I)}(t) e^{\frac{iH^{(0)}t}{\hbar}} \quad (9)$$

Note that if considered with respect to $H^{(0)}$, $\rho^{(I)}(t)$ must be interpreted as corresponding to the Heisenberg picture. This is the reason why, henceforth, we will state that the operators are taken in the Heisenberg picture. Eq. (9) gives us the time evolution of $\rho^{(I)}(t)$ as

$$\begin{aligned} i\hbar \partial_t \rho(t) &= \left[H^{(0)}(t), \rho(t) \right] + i\hbar e^{-\frac{iH^{(0)}t}{\hbar}} \partial_t \rho^{(I)}(t) e^{\frac{iH^{(0)}t}{\hbar}} \\ &\Rightarrow e^{\frac{iH^{(0)}t}{\hbar}} [V(t), \rho(t)] e^{-\frac{iH^{(0)}t}{\hbar}} = i\hbar \partial_t \rho^{(I)}(t) \\ &\Rightarrow i\hbar \partial_t \rho^{(I)}(t) = \left[V^{(I)}(t), \rho^{(I)}(t) \right], \end{aligned} \quad (10)$$

where we have used Eq. (7). The formal solution of the above differential equation is given by

$$\rho^{(I)}(t) = \rho^{(0)} - \frac{i}{\hbar} \int_{-\infty}^t dt' \left[V^{(I)}(t'), \rho^{(I)}(t') \right]. \quad (11)$$

Going back to the Schrödinger picture, the solution above leads to

$$\rho(t) = \rho^{(0)} - \frac{i}{\hbar} \int_{-\infty}^t dt' e^{\frac{-iH^{(0)}(t-t')}{\hbar}} [V(t'), \rho(t')] e^{\frac{iH^{(0)}(t-t')}{\hbar}}, \quad (12)$$

which can be solved recursively order by order by generating a systematic expansion with respect to $V(t)$. At zeroth order, we have $\rho(t) = \rho^{(0)} + \mathcal{O}(V(t))$. At first order, we insert the zeroth order result, and obtain

$$\begin{aligned} \rho(t) &= \rho^{(0)} - \frac{i}{\hbar} \int_{-\infty}^t dt' e^{\frac{-iH^{(0)}(t-t')}{\hbar}} [V(t'), \rho^{(0)}] e^{\frac{iH^{(0)}(t-t')}{\hbar}} \\ &\quad + \mathcal{O}(V^2(t)) \\ &= \rho^{(0)} - \frac{i}{\hbar} \int_{-\infty}^t dt' [V^{(I)}(t'), \rho^{(0)}] + \mathcal{O}(V^2(t)), \end{aligned} \quad (13)$$

which is the regime of linear response. Hence, it follows from Eq. (6) that

$$\begin{aligned} \langle \mathcal{O} \rangle_t &= \text{Tr}[\rho^{(0)} \mathcal{O}] - \frac{i}{\hbar} \int_{-\infty}^t dt' \text{Tr}[[V(t'), \rho^{(0)}] \mathcal{O}^{(I)}(t)] \\ &= \langle \mathcal{O} \rangle - \frac{i}{\hbar} \int_{-\infty}^t dt' \text{Tr}[[\mathcal{O}^{(I)}(t), V(t')] \rho^{(0)}] \\ &= \langle \mathcal{O} \rangle - \frac{i}{\hbar} \int_{-\infty}^t dt' \langle [\mathcal{O}^{(I)}(t), V(t')] \rangle, \end{aligned} \quad (14)$$

where the symbol $\langle \dots \rangle$ stands for an equilibrium expectation value with respect to the Hamiltonian $H^{(0)}$.

Using the definition of the retarded correlator for two operators \mathcal{A}_1 and \mathcal{A}_2 as

$$\langle \langle \mathcal{A}_1^{(I)}(t); \mathcal{A}_2^{(I)}(t') \rangle \rangle = \frac{i}{\hbar} \Theta(t-t') \langle [\mathcal{A}_1^{(I)}(t), \mathcal{A}_2^{(I)}(t')] \rangle, \quad (15)$$

Eq. (14) can finally be expressed as

$$\langle \mathcal{O} \rangle_t = \langle \mathcal{O} \rangle - \int_{-\infty}^{\infty} dt' \langle \langle \mathcal{O}^{(I)}(t); V^{(I)}(t') \rangle \rangle. \quad (16)$$

which demonstrates the core fact that the linear response of a quantum system is characterized by retarded Green's functions. This is indeed an extremely useful result, because the inherently nonequilibrium observable $\langle \mathcal{O} \rangle_t$ has been expressed as a correlation function of the system in equilibrium. The physical reason for this remarkable result is that the effects of the interactions between the excitations created in the nonequilibrium state show up at second order in the perturbation and, hence, not included in linear response.

2. The Kubo identity and the retarded Green's function in the frequency domain

We consider an external and time-dependent perturbation of the form

$$V(t) = -\mathcal{B} F(t), \quad (17)$$

where \mathcal{B} is an of the theory and $F(t)$ is a classical time-dependent function. For an observable \mathcal{A} , Eq. (16) yields the linear response relation

$$\langle \mathcal{A} \rangle_t = \langle \mathcal{A} \rangle + \int_{-\infty}^{\infty} dt' G_{\mathcal{A}\mathcal{B}}^R(t-t') F(t') \quad (18)$$

where

$$\begin{aligned} G_{\mathcal{A}\mathcal{B}}^R(t-t') &\equiv \langle \langle \mathcal{A}(t); \mathcal{B}(t') \rangle \rangle \\ &= \frac{i}{\hbar} \Theta(t) \langle [\mathcal{A}(t), \mathcal{B}(t')] \rangle, \end{aligned} \quad (19)$$

is the retarded Green's function¹ for the operators $\mathcal{A}(t)$ and $\mathcal{B}(t')$. Here, the time-dependent observables have been expressed in the Heisenberg representation of $H^{(0)}$ (as explained earlier).

We will need to use the Kubo identity

$$\frac{i}{\hbar} [\mathcal{O}(t'), \rho^{(0)}] = \rho^{(0)} \int_0^\beta d\tau \dot{\mathcal{O}}(t)|_{t=t'-i\hbar\tau}, \quad (20)$$

where an overhead dot indicates total derivative with respect to t and, for a general operator \mathcal{O} in the Schrödinger picture, the Heisenberg picture version $\mathcal{O}(t)$ is defined by

$$\mathcal{O}(t) = e^{\frac{iH^{(0)}t}{\hbar}} \mathcal{O} e^{-\frac{iH^{(0)}t}{\hbar}}. \quad (21)$$

The Kubo identity can be proved easily via the following steps, starting from the right-hand-side of Eq. (20):

$$\begin{aligned} \rho^{(0)} \int_0^\beta d\tau \frac{d\mathcal{O}(t)}{dt} \Big|_{t=t'-i\hbar\tau} &= \frac{i\rho^{(0)}}{\hbar} \int_0^\beta d\tau \frac{d}{d\tau} \mathcal{O}(t' - i\hbar\tau) \\ &= \frac{i\rho^{(0)}}{\hbar} [\mathcal{O}(t' - i\hbar\beta) - \mathcal{O}(t')] \\ &= \frac{i}{\hbar} \left[\frac{e^{-\beta H^{(0)}}}{\mathcal{Z}(\beta)} e^{H^{(0)}\beta} \mathcal{O}(t') e^{-H^{(0)}\beta} - \rho^{(0)} \mathcal{O}(t') \right] \\ &= \frac{i}{\hbar} [\mathcal{O}(t') \rho^{(0)} - \rho^{(0)} \mathcal{O}(t')] = \frac{i}{\hbar} [\mathcal{O}(t'), \rho^{(0)}]. \end{aligned} \quad (22)$$

Using Eq. (20) in Eq. (19), we get

$$\begin{aligned} G_{\mathcal{A}\mathcal{B}}^R(t-t') &\equiv \frac{i}{\hbar} \Theta(t) \text{Tr}[\rho^{(0)} [\mathcal{A}(t), \mathcal{B}(t')]] \\ &= -\frac{i}{\hbar} \Theta(t-t') \text{Tr}[\rho^{(0)} \mathcal{B}(t') \mathcal{A}(t) - \mathcal{B}(t') \rho^{(0)} \mathcal{A}(t)] \\ &= -\Theta(t-t') \text{Tr} \left[\frac{i}{\hbar} [\rho^{(0)}, \mathcal{B}(t')] \mathcal{A}(t) \right] \\ &= \Theta(t-t') \text{Tr}[\rho^{(0)} \int_0^\beta d\tau \dot{\mathcal{B}}(t' - i\hbar\tau) \mathcal{A}(t)] \\ &= \Theta(t-t') \int_0^\beta d\tau \langle \dot{\mathcal{B}}(t' - i\hbar\tau) \mathcal{A}(t) \rangle. \end{aligned} \quad (23)$$

¹ An alternate convention, differing by an overall sign, appears in the literature (e.g., in Ref. [111]) for the definition of the retarded Green's function, and $\Theta(t)$ is Heaviside step function. However, the convention adopted here is much more standard and is the common choice in condensed-matter physics [58].

Further simplifying the expressions, we can write

$$\begin{aligned} G_{\mathcal{A}\mathcal{B}}^R(t) &= \Theta(t) \int_0^\beta d\tau \langle \dot{\mathcal{B}}(-i\hbar\tau) \mathcal{A}^{(I)}(t) \rangle \\ &= \Theta(t) \int_0^\beta d\tau \langle \dot{\mathcal{B}}(-t - i\hbar\tau) \mathcal{A} \rangle. \end{aligned} \quad (24)$$

We now go to the Fourier space, defining the Fourier transform $\tilde{G}_{\mathcal{A}\mathcal{B}}^R(\omega) \equiv \int_{-\infty}^{\infty} dt e^{i\omega_+ t} G_{\mathcal{A}\mathcal{B}}^R(t)$, where $\omega_+ = \omega + i0^+$. The part 0^+ denotes an infinitesimally small positive number, which is incorporated in order to ensure the correct physical result, namely the retarded correlator decays at large times. The Fourier transform evaluates to

$$\begin{aligned} \tilde{G}_{\mathcal{A}\mathcal{B}}^R(\omega) &= \int_0^\infty dt \int_0^\beta d\tau e^{i\omega_+ t} \langle \dot{\mathcal{B}}(-t - i\hbar\tau) \mathcal{A} \rangle \\ &= g_1 + g_2, \\ g_1 &= \frac{1}{i\omega_+} \int_0^\beta d\tau e^{i\omega_+ t} \langle \dot{\mathcal{B}}(-t - i\hbar\tau) \mathcal{A} \rangle \Big|_{t=0}^{t=\infty}, \\ g_2 &= -\frac{1}{i\omega_+} \int_0^\infty dt \int_0^\beta d\tau e^{i\omega_+ t} \frac{d}{dt} \langle \dot{\mathcal{B}}(-t - i\hbar\tau) \mathcal{A} \rangle. \end{aligned} \quad (25)$$

Let us first analyze the second term, which simplifies to

$$\begin{aligned} -i\omega_+ g_2 &= \int_0^\infty dt e^{-i\omega_+ t} \text{Tr} \left[\left\{ \rho^{(0)} \int_0^\beta d\tau \frac{d}{dt} \dot{\mathcal{B}}(t - i\hbar\tau) \right\} \mathcal{A} \right] \\ &= \frac{i}{\hbar} \int_0^\infty dt e^{-i\omega_+ t} \text{Tr} [[\dot{\mathcal{B}}(t), \rho^{(0)}] \mathcal{A}] \\ &= \frac{i}{\hbar} \int_0^\infty dt e^{i\omega_+ t} \text{Tr} [[\rho^{(0)}, \dot{\mathcal{B}}] \mathcal{A}(t)] \\ &= \frac{i}{\hbar} \int_0^\infty dt e^{i\omega_+ t} \text{Tr} [\rho^{(0)} \dot{\mathcal{B}} \mathcal{A}(t) - \rho^{(0)} \mathcal{A}(t) \dot{\mathcal{B}}] \\ &= \int_{-\infty}^\infty dt e^{i\omega_+ t} \frac{(-i)}{\hbar} \Theta(t) \langle [\mathcal{A}(t), \dot{\mathcal{B}}] \rangle \\ &= -\tilde{G}_{\mathcal{A}\dot{\mathcal{B}}}^R(\omega), \end{aligned} \quad (26)$$

where

$$\begin{aligned} G_{\mathcal{A}\dot{\mathcal{B}}}^R(t-t') &\equiv \frac{i}{\hbar} \Theta(t) \langle [\mathcal{A}(t), \dot{\mathcal{B}}(t')] \rangle, \\ \tilde{G}_{\mathcal{A}\dot{\mathcal{B}}}^R(\omega) &= \int_{-\infty}^\infty dt e^{i\omega_+ t} G_{\mathcal{A}\dot{\mathcal{B}}}^R(t). \end{aligned} \quad (27)$$

As for the first term g_1 , the part evaluated at $t = \infty$ must go to zero, as that is the boundary condition, which we have ensured by including convergence factor ($= -0^+ t$) in the argument of the exponential. Thus, $g_1 = \frac{1}{i\omega_+} \chi_{\ell_1 \ell_2}$, where

$$\chi_{\mathcal{A}\dot{\mathcal{B}}} = \int_0^\beta d\tau \langle \dot{\mathcal{B}}(-i\hbar\tau) \mathcal{A} \rangle = \lim_{\omega \rightarrow 0} \tilde{G}_{\mathcal{A}\dot{\mathcal{B}}}^R(\omega), \quad (28)$$

which is called the static susceptibility. Hence, the final expressions for the retarded Green's function in the Fourier space reduces to

$$\tilde{G}_{\mathcal{A}\mathcal{B}}^R(\omega) = \frac{1}{i\omega_+} \left[\tilde{G}_{\mathcal{A}\dot{\mathcal{B}}}^R(\omega) - \chi_{\mathcal{A}\mathcal{B}} \right]. \quad (29)$$

3. Conductivity tensor

Let us consider a system of charged particles (which are electrons in usual condensed matter systems) subjected to an external spatially homogeneous time-dependent electric field $\mathbf{E}(t)$ [cf. Eq. (4)]. The electric field induces a current, and the conductivity tensor is the linear response coefficient. For definiteness, let us consider electrons to be the charge carriers, each of which has charge e .

Let us first define the electric current density operator. In the position space representation for the equilibrium Hamiltonian of the system (which is expressed in terms of the fermionic quantum fields), we make the replacement $-i\hbar\partial_{r^p} \rightarrow -i\hbar\partial_{r^p} - \frac{e}{c}A^p$, which we denote by $\tilde{H}^{(0)}[\mathbf{A}]$. The components of \mathbf{J} is then derived as the functional derivatives

$$J_p = -\frac{\delta \tilde{H}^{(0)}[\mathbf{A}]}{\delta A^p}. \quad (30)$$

However, for a parabolic spectrum, in addition to the \mathbf{A} -independent term, this generates a linear-in- \mathbf{A} term for a parabolic spectrum. This necessitates gauge-fixing while finding the final expressions. A simpler alternate way is to define the current operator using the relation $\mathbf{J} = \dot{\mathcal{P}} = \frac{i}{\hbar} [H^{(0)}, \mathcal{P}]$, where \mathcal{P} is the electrical dipole moment operator, which couples to the external electric field. We can express \mathcal{P} as $\int d^d \mathbf{r} \mathbf{r} n_c$, where n_c is the electric charge density operator. Using this line of argument, we need to set

$$V(t) = -\mathcal{P} \cdot \mathbf{E}(t). \quad (31)$$

We can now use Eqs. (18) and (19) by setting $\mathcal{A} = J_p$, $\mathcal{B} = \mathcal{P}_q$, and $F(t) = E_q(t) = E_q^{(0)} e^{-i\omega_+ t}$. The identity $\dot{\mathcal{P}}_q = J_q$ leads to

$$\chi_{J_p \dot{\mathcal{P}}_q}(t) \equiv \chi_{J_p J_q}(t) = \frac{i}{\hbar} \Theta(t) \langle [J_p(t), J_q] \rangle. \quad (32)$$

Since the conductivity in the temporal space is defined as

$$\langle J_p \rangle_t = \int_{-\infty}^\infty dt' \sigma_{pq}^{\text{temp}}(t-t') E_q(t'), \quad (33)$$

and Eq. (18) results in (since the average current in the equilibrium distribution is zero)

$$\langle J_p \rangle_t = \int_{-\infty}^\infty dt' G_{J_p \mathcal{P}_q}^R(t-t') E_q(t'), \quad (34)$$

we conclude that

$$\sigma_{pq}^{\text{temp}}(t-t') = G_{J_p \mathcal{P}_q}^R(t-t'). \quad (35)$$

Fourier transforming to the frequency space, and using (29), we finally obtain the Fourier-space conductivity as

$$\sigma_{pq}(\omega) \equiv \tilde{G}_{J_p \mathcal{P}_q}^R(\omega) = \frac{-i}{\omega_+} \left[\tilde{G}_{J_p J_q}^R(\omega) - \chi_{J_p J_q} \right]. \quad (36)$$

We point out that yet another widely used procedure [110, 112] is to express \mathbf{E} in terms of the scalar and vector potentials and, then, using the continuity equation

$$\partial_t n_c(\mathbf{r}, t) = -\nabla \cdot \mathbf{J}(\mathbf{r}, t). \quad (37)$$

B. Memory matrix formalism

The memory matrix formalism is the second formalism we are going to focus on in this review, which is a powerful technique for describing transport in strongly correlated systems without quasiparticles. In this subsection, we discuss the procedure to compute the response at finite temperatures, mainly following the treatment in Refs. [57, 58].

The simplest framework of describing transport without reference to quasiparticles is, in fact, hydrodynamics, which has been known for a very long time. Although hydrodynamics was synonymous with fluid dynamics before the twentieth century, the modern understanding of hydrodynamics is that it describes the long-wavelength and long-time-scale dynamics of an interacting classical or quantum system close to thermal equilibrium, when there is a small number of conserved quantities [113]. In other words, the key assumption of hydrodynamics is that the field theory has locally reached a thermal equilibrium. A more generic treatment allows for some of these conserved quantities to decay on long time scales, while still retaining the nomenclature of “hydrodynamics” [58]. The only requirement for applying this generalized treatment is that the list of such conserved quantities must be finite. Although this requirement cannot be fulfilled in Fermi liquids, because we have occupation numbers of the long-lived quantities at every single wavevector (which forms an infinite set). However, for NFLs, it is believed that generic higher dimensional theories do not admit infinite families of nearly-conserved quantities at strong coupling, and, therefore, the requirement is easily satisfied.

Despite the fact that the effective theory of hydrodynamics provides the relaxation of an interacting classical or quantum system towards thermal equilibrium, without any reference to the existence of quasiparticles, it is important to note that hydrodynamics is an incomplete description. This implies that although hydrodynamics provides a universal framework, via a set of constraints that any reasonable (and, at least, approximately translation-invariant) quantum field theory at finite density and temperature must obey, it does not give us any specific values or temperature-dependence for the microscopic coefficients. The memory matrix approach provides a way of obtaining the microscopic coefficients. In particular, one does not need to add a phenomenological momentum relaxation time, as required in hydrodynamics, as this coefficient can be computed separately using the memory matrix formalism. Although, in principle, the memory matrix technique is an exact microscopic calculation, its practical usefulness stems from the fact that it can be efficiently approximated in a hydrodynamic regime where there are only a small handful of quantities which do not quickly relax to thermal equilibrium.

As discussed in the introduction, the memory matrix technique is essentially employing the coarse-graining procedure to obtain the time-evolution of the slow/long-lived (hydrodynamic) modes by “integrating out” the fast (microscopic) modes. This approach was introduced by Mori [52, 53], Zwanzig [54, 55], and developed further by Götze and Wölfle [56, 57] more than half a century ago. Zwanzig separated the ensemble density into relevant and an ir-

relevant parts by means of a projection, solved the latter part formally in terms of the former one, and substituted the solution back into the equation for the relevant part [52]. This exact transformation is particularly suitable for integrating out the fast modes (i.e., modes having fast variations in time) [55]. Following the earlier arguments, the method works best when quasiparticles are not long-lived, and the only conserved (or approximately conserved) quantities are charge, energy, and momentum. In the last two decades, this computational tool has become a method of choice for studying transport in NFL phases arising in one-dimensional [114, 115] and higher-dimensional systems [58, 70, 71, 75–77, 116–122], as well as strongly-interacting quantum field theories in the context of using gauge-gravity duality [123–127].

Let us now briefly outline the notations required in applying the memory matrix framework. In the following, we will set \hbar and k_B to unity, agreeing to use natural units. Let us consider the set of linear operators $\{\mathcal{A}, \mathcal{B}, \mathcal{C}, \dots\}$ in a time-translation invariant theory. The space of linear operators acting on a Hilbert space is called Liouville space. When dealing with a complicated quantum system, we are usually neither interested in nor capable of describing the time evolution of all its microscopic properties. Rather, most of the times, we want to compute to determine the linear response, which require the knowledge of the dynamics of only a small set of selected (“relevant”) observables. These relevant observables, together with the identity operator, span a (relatively small) subspace of the Liouville space, which is known as the *level of description* [128]. Consequently, the dynamics is projected onto the level of description, which yields closed equations of motion for the relevant observables only (although it is, in general, no longer Markovian).

The detection and systematic exploitation of a separation of time scales is the basic practical merit of the projection-operator method [128]. A simple example to illustrate this is the Brownian motion of a massive particle within a fluid of small molecules. This process consists of damping on a macroscopic scale due to the viscosity of the fluid, and fast vibrations due to stochastic residual forces. Both the processes are caused by collisions between the particle and the fluid molecules, but they take place on different time scales — the damping process is much more relevant for the observable “position of the particle”, compared to the vibrations, since the latter vanish when averaged over time. However, only if the *relevant processes* are filtered out, we can neglect the fast modes.

1. Memory function formalism

A necessary condition for the definition of a projector is the existence of a scalar product within the Liouville space. There are multiple possibilities to do so. Here, we use the definition put forward by Mori [52], using the inner product

$$\begin{aligned} \Upsilon_{\mathcal{A}\mathcal{B}}(t) &\equiv (\mathcal{A}(t)|\mathcal{B}(0)), \\ (\mathcal{A}(t)|\mathcal{B}(0)) &\equiv \int_0^\beta d\lambda \langle \mathcal{A}^\dagger(t) \mathcal{B}(i\lambda) \rangle, \end{aligned} \quad (38)$$

with averages over thermal and quantum fluctuations denoted by the symbol $\langle \dots \rangle$. Here, L is the Liouvillian (or Liouville operator), defined by

$$L \circ = [H^{\text{tot}}(t), \circ] = [H^{(0)}, \circ] + [V(t), \circ], \quad (39)$$

and $|\mathcal{A}(t)\rangle \equiv e^{iLt} |\mathcal{A}(0)\rangle$. Note that the usual convention is to denote $\mathcal{A}(0)$ simply by \mathcal{A} — hence, we will use these two alternate notations interchangeably. The expression follows from the fact that, when written in terms of the Liouvillian, the Heisenberg equation of motion for \mathcal{A} reads

$$\frac{d\mathcal{A}(t)}{dt} = iL\mathcal{A} \Rightarrow \mathcal{A}(t) = e^{iLt} \mathcal{A}(0). \quad (40)$$

Rather than working in the time domain, we will take Laplace transforms to work in the frequency domain. The Laplace transform of a function $F(t)$ is defined by

$$\tilde{F}(z) = \int_0^\infty dt e^{izt} F(t). \quad (41)$$

Furthermore, we need the counterpropagator

$$\mathcal{R}(z) = \int_0^\infty dt e^{izt} e^{iLt} = \frac{i}{z-L}, \quad (42)$$

where $\text{Im}(z) > 0$. We denote the Laplace-transformed correlation function in Eq. (38) by the symbol $\tilde{\Upsilon}_{\mathcal{A}\mathcal{B}}(z)$, such that

$$\begin{aligned} \tilde{\Upsilon}_{\mathcal{A}\mathcal{B}}(z) &\equiv \int_0^\infty dt e^{izt} \Upsilon_{\mathcal{A}\mathcal{B}}(t) \\ &= \int_0^\infty dt e^{izt} (A(0) e^{iLt} |B(0)\rangle) \\ &= \int_0^\infty dt e^{izt} (A(0) | e^{-iLt} B(0)\rangle) \\ &= (A(0) | \mathcal{R}(z) B(0)\rangle). \end{aligned} \quad (43)$$

By using $\mathcal{R}(z) = [L\mathcal{R}(z) - L\mathcal{R}(0)]/z$, we obtain

$$\tilde{\Upsilon}_{\mathcal{A}\mathcal{B}}(z) = \frac{1}{iz} \left[\tilde{G}_{\mathcal{A}\mathcal{B}}^{\text{R}}(z) - \tilde{G}_{\mathcal{A}\mathcal{B}}^{\text{R}}(i0) \right], \quad (44)$$

where $\tilde{G}_{\mathcal{A}\mathcal{B}}^{\text{R}}(z)$ is the Laplace transform of the retarded Green's function (in real space and time) is defined as

$$G_{\mathcal{A}\mathcal{B}}^{\text{R}}(t, \mathbf{r}) \equiv i\Theta(t) \langle [\mathcal{A}(t, \mathbf{r}), \mathcal{B}(0, \mathbf{0})] \rangle. \quad (45)$$

This is the same as Eq. (19), except that the position-dependence has been suppressed in the former equation, since there we were dealing with a spatially uniform perturbation. Henceforth, we will suppress the position/momentum dependence of the retarded Green's functions [as already done in Eq. (44)], as in this entire review, we are only interested in the response functions evaluated at zero momentum. Here, we will only be computing thermoelectric transport coefficients, for which $\tilde{G}_{\mathcal{A}\mathcal{B}}^{\text{R}}(\omega \rightarrow 0) \sim i\omega \mathfrak{s}_{\mathcal{A}\mathcal{B}}$, where $\mathfrak{s}_{\mathcal{A}\mathcal{B}}$ is the generalized conductivity between the operators \mathcal{A} and \mathcal{B} . Since $\mathfrak{s}_{\mathcal{A}\mathcal{B}}$ is strictly finite, we have $\tilde{G}_{\mathcal{A}\mathcal{B}}^{\text{R}}(i0) = 0$ and, hence, can be omitted in the rest of the discussions. Therefore, in this context, $\tilde{\Upsilon}_{\mathcal{A}\mathcal{B}}(z)$ turns out to be equal to $\mathfrak{s}_{\mathcal{A}\mathcal{B}}$.

After performing some formal manipulations on the Hilbert space of operators lead to

$$\begin{aligned} \mathfrak{s}_{\mathcal{A}\mathcal{B}}(z) &\equiv \tilde{\Upsilon}_{\mathcal{A}\mathcal{B}}(z) \\ &= \chi_{\mathcal{A}\mathcal{C}} \left[\frac{1}{M(z) + N - iz\chi} \right]_{\mathcal{C}\mathcal{D}} \chi_{\mathcal{D}\mathcal{B}}, \end{aligned} \quad (46)$$

where χ is the matrix with elements

$$\chi_{\mathcal{A}\mathcal{B}} = (\mathcal{A}(0) | \mathcal{B}(0)\rangle). \quad (47)$$

$\chi_{\mathcal{A}\mathcal{B}}$ is known as the static susceptibility between the operators \mathcal{A} and \mathcal{B} [same as Eq. (28)]. The symbol M stands for the so-called memory matrix, whose components are defined as

$$M_{\mathcal{A}\mathcal{B}}(z) = i \left(\dot{\mathcal{A}} \left| \mathcal{Q} \frac{1}{z - \mathcal{Q}L\mathcal{Q}} \mathcal{Q} \right| \dot{\mathcal{B}} \right), \quad (48)$$

where

$$\mathcal{P} = \sum_{\mathcal{A}\mathcal{B}} |\mathcal{A}(0)\rangle \chi_{\mathcal{A}\mathcal{B}}^{-1} \langle \mathcal{B}(0)|, \quad \mathcal{Q} = \mathbb{I} - \mathcal{P}, \quad (49)$$

and the matrix N has the components

$$N_{\mathcal{A}\mathcal{B}} \equiv \chi_{\mathcal{A}\dot{\mathcal{B}}} = -\chi_{\dot{\mathcal{A}}\mathcal{B}}. \quad (50)$$

Clearly, $N_{\mathcal{A}\mathcal{B}}$ is antisymmetric, and it vanishes identically in a time-reversal-invariant system if the operators \mathcal{A} and \mathcal{B} transform identically under time reversal.

We implement the above formula by projecting onto a basis of nearly-conserved operators, which we denote by $\{\xi_i\}$, with a long relaxation time compared to microscopic timescales. These conservation laws are related to symmetries in the model that protect these operators from decaying — a *small amount of symmetry-breaking* cause these operators to become nearly conserved (rather than completely conserved). With this in mind, we define the projection operator \mathcal{P} [defined above in Eq. (49)] to project onto the slow-mode basis as [57]

$$\mathcal{P} = \sum_{ij} |\xi_i(0)\rangle \chi_{\xi_i \xi_j}^{-1} \langle \xi_j(0)|. \quad (51)$$

Therefore, the complement operator \mathcal{Q} projects out of the space spanned by these nearly-conserved observables. We want to extract from the Liouville operator that part which changes a given ξ_{i_0} (for $i = i_0$) only in the subspace spanned by $\{\xi_i\}$. Since $\mathcal{P} + \mathcal{Q} = \mathbb{I}$, we use the form $L = L\mathcal{P} + L\mathcal{Q}$. By using the operator identity [57]

$$\frac{1}{\mathcal{A} + \mathcal{B}} = \frac{1}{\mathcal{A}} - \frac{1}{\mathcal{A}} \mathcal{B} \frac{1}{\mathcal{A} + \mathcal{B}}, \quad (52)$$

and using the fact that \mathcal{P} acts as an identity operator in the space $\{\xi_i\}$, we get

$$\begin{aligned} \tilde{\Upsilon}_{\xi_i \xi_j}(z) &\equiv (\xi_i(0) | \frac{i}{z-L} | \xi_j(0)\rangle) \\ &= (\xi_i(0) | \frac{i}{z-L\mathcal{Q} - L\mathcal{P}} | \xi_j(0)\rangle) \\ &= (\xi_i(0) | \left[\frac{i}{z-L\mathcal{Q}} + \frac{i}{z-L\mathcal{Q}} L\mathcal{P} \frac{1}{z-L} \right] | \xi_j(0)\rangle). \end{aligned} \quad (53)$$

For the first term, we first observe that

$$\frac{i}{z-L\mathcal{Q}} = \frac{i}{z} \left[1 + \frac{1}{z}L\mathcal{Q} + \frac{1}{z^2}L\mathcal{Q}L\mathcal{Q} + \dots \right], \quad (54)$$

which shows that, except the first term, each term ends with the operator \mathcal{Q} , and $\mathcal{Q}|\xi_i\rangle = 0$. As for the second term in Eq. (53), we observe that

$$\begin{aligned} \mathcal{P} \frac{i}{z-L} |\xi_j(0)\rangle &= |\xi_{j'}(0)\rangle \chi_{\xi_{i'}\xi_{j'}}^{-1} (\xi_{j'}(0)| \frac{i}{z-L} |\xi_j(0)\rangle) \\ &= |\xi_{i'}(0)\rangle \chi_{\xi_{i'}\xi_{j'}}^{-1} \tilde{\Upsilon}_{\xi_{j'}\xi_j}(z). \end{aligned} \quad (55)$$

Putting these results together, Eq. (53) evaluates to

$$\begin{aligned} &\tilde{\Upsilon}_{\xi_i\xi_j}(z) - \frac{i}{z} \chi_{\xi_i\xi_j} \\ &= (\xi_i(0)| \frac{1}{z-L\mathcal{Q}} L |\xi_{i'}(0)\rangle) \chi_{\xi_{i'}\xi_{j'}}^{-1} \tilde{\Upsilon}_{\xi_{j'}\xi_j}(z) \\ &= (\xi_i| \left[\frac{1}{z} + \frac{1}{z}L\mathcal{Q} \frac{1}{z-L\mathcal{Q}} \right] L |\xi_{i'}\rangle) \chi_{\xi_{i'}\xi_{j'}}^{-1} \tilde{\Upsilon}_{\xi_{j'}\xi_j}(z) \\ &= \frac{1}{z} \left[(\xi_i| L |\xi_{i'}\rangle) + (\xi_i| L\mathcal{Q} \frac{1}{z-L\mathcal{Q}} \mathcal{Q}L |\xi_{i'}\rangle) \right] \\ &\quad \times \chi_{\xi_{i'}\xi_{j'}}^{-1} \tilde{\Upsilon}_{\xi_{j'}\xi_j}(z). \end{aligned} \quad (56)$$

The step can be proven with the help of a geometric series (similar to Eq. (54)), and using the identity $\mathcal{Q}^2 = \mathcal{Q}$.

2. Generalized conductivity tensors in the absence of magnetic fields

Our goal is to compute the conductivity tensors at zero momentum, but finite frequency in general. To start with, we want to consider the case with zero magnetic field, which means that the time-reversal symmetry-breaking matrix N will vanish.

In NFLs, the kinematics of the almost-conserved quantities is entirely different from Fermi liquid theory, and the Wiedemann-Franz law is expected not to hold, even approximately [75]. Since an infinite collection of conserved densities does not exist in the effective low-energy theory, it follows that generically the total electrical and heat currents (unlike in a Fermi liquid). The only conserved quantities are the momenta, up to the effect of irrelevant or weak marginal operators. The conservation of momentum, up to effects that are small at low energies, is a key assumption that allows the memory matrix method to work. While there are strong interactions in an NFL, it is still possible that there emerges a decoupling of the excitations into patches in the momentum space, for example a critical Fermi surface in $(2+1)$ -dimensions [11, 13, 22, 31]. For such cases, there exist a family of conserved momenta momentum vectors. However, here we are interested in NFLs arising at nodal points (with no patch structure), which implies that we will focus on scenarios when there is only one almost-conserved vector operator in the effective low-energy theory.

In the systems we are interested in, the total momentum vector operator \mathbf{P} is relaxed on a much longer timescale

than all other quantities, including the currents [75]. Nevertheless, our discussion can easily be adapted to cases in which the electric current is equal to the momentum. The only general requirement for the results to hold is that there exists only one almost-conserved vector operator. For simplicity, we will assume that the system is spatially isotropic, such that all the diagonal components of M are equal and all its transverse components vanish (i.e., $M_{P_p P_q} \propto \delta_{pq}$).

The dc conductivity determines the dissipation due to an arbitrarily low-frequency current being driven through the system. In a translationally invariant field theory at finite density, such that the only conserved vector quantity is the total momentum, the dc conductivity tensors diverge [129, 130]. Intuitively, the conductivity diverges because the current operator has some overlap with the momentum operator, which is conserved. To remedy the infinite dc conductivity result, we perturb this theory by an irrelevant operator that breaks translational invariance, so the infrared is still described by the original fixed point. This renders the total momentum a nearly-conserved operator.

Some standard mechanisms that can cause momentum relaxation in a transport theory are Umklapp processes, coupling to phonons, and impurity scattering. Umklapp scattering is usually exponentially suppressed at low temperatures and, since it depends on details associated with the shape of the underlying Fermi surface of a quantum system, its contribution for transport is expected to be non-universal. On the other hand, the universal contribution for transport are expected to originate from either disorder effects or coupling to a phonon bath. Moreover, conventional wisdom suggests that scattering of charge carriers by phonons turns out to be most effective as a relaxation mechanism for many systems only at high temperatures, since they tend to be generally suppressed at low-enough temperatures. Because of this, we will choose to concentrate mainly on impurity scattering as the main mechanism that causes momentum relaxation in the transport theory.

To implement momentum relaxation induced by impurity scatterings, we will add a weak random impurity potential that couples to the fermionic density in a system with N_f fermion flavours as a quenched disorder (i.e., with no time evolution). If the fermionic field is denoted as $\psi(t, \mathbf{r})$, we need to add the impurity action [131]

$$S_{\text{imp}} = \int dt d^d \mathbf{r} W(\mathbf{r}) \psi^\dagger(t, \mathbf{r}) \psi(t, \mathbf{r}). \quad (57)$$

It is common to take $W(\mathbf{r})$ to be a zero-mean Gaussian random function, with the mean and the variance obeying [124]

$$\overline{W(\mathbf{r})} = 0, \quad \overline{W(\mathbf{r})W(\mathbf{r}')^*} = W_0^2 \delta^d(\mathbf{r} - \mathbf{r}'), \quad (58)$$

where the overline denotes disorder averaging, and W_0^2 represents the average magnitude square of the random potential experienced by the fermionic fields. We will work to order W_0^2 .

To apply the memory matrix method explained in the previous subsection, we need to calculate the time dependence of the slowly-varying operator P_p using the total

Hamiltonian $H^{(0)} + H_{\text{imp}}$, where

$$\begin{aligned} H_{\text{imp}} &= - \int d^d \mathbf{r} W(\mathbf{r}) \mathcal{O}(t, \mathbf{r}), \\ \mathcal{O}(t, \mathbf{r}) &\equiv \psi_i^\dagger(t, \mathbf{r}) \psi_i(t, \mathbf{r}). \end{aligned} \quad (59)$$

is the part of the total Hamiltonian representing the contribution from disorder. The time evolution of P_p is given by $\dot{P}_p = i [H^{(0)} + H_{\text{imp}}, P_p]$, which, in the position space representation, reduces to

$$\begin{aligned} \dot{P}_p(t, \mathbf{r}) &= i \int d^d \mathbf{r}' W(\mathbf{r}') [P_p(\mathbf{r}), \mathcal{O}(t, \mathbf{r}')] \\ &= \int d^d \mathbf{r}' \delta^d(\mathbf{r} - \mathbf{r}') W(\mathbf{r}') \partial_{r_p} \mathcal{O}(t, \mathbf{r}') \\ &= W(\mathbf{r}) \partial_{r_p} \mathcal{O}(t, \mathbf{r}). \end{aligned} \quad (60)$$

For convenience, we define

$$\begin{aligned} F_{\dot{P}_p \dot{P}_q}(t, \mathbf{r}, \tilde{\mathbf{r}}) &= \overline{W(\mathbf{r}) W(\tilde{\mathbf{r}})} \langle [\partial_{r_p} \mathcal{O}(t, \mathbf{r}), \partial_{\tilde{r}_q} \mathcal{O}(0, \tilde{\mathbf{r}})] \rangle \\ &= -W_0^2 \delta^d(\mathbf{r} - \tilde{\mathbf{r}}) \\ &\quad \times \int \frac{d^d \mathbf{k} d^d \mathbf{k}'}{(2\pi)^{2d}} k_p k'_q [\mathcal{O}(t, \mathbf{k}), \mathcal{O}(0, \mathbf{k}')] e^{i(\mathbf{k} + \mathbf{k}') \cdot \mathbf{r}}. \end{aligned} \quad (61)$$

Taking a Fourier transform and evaluating the zero momenta parts, we get

$$\begin{aligned} \tilde{F}_{\dot{P}_p \dot{P}_q}(t, \tilde{\mathbf{k}}, \tilde{\mathbf{k}}') \Big|_{\tilde{\mathbf{k}} = \tilde{\mathbf{k}}' = 0} &= -W_0^2 \int d^d \mathbf{r} d^d \tilde{\mathbf{r}} \delta^d(\mathbf{r} - \tilde{\mathbf{r}}) \\ &\quad \times \int \frac{d^d \mathbf{k} d^d \mathbf{k}'}{(2\pi)^{2d}} k_p k'_q [\mathcal{O}(t, \mathbf{k}), \mathcal{O}(0, \mathbf{k}')] e^{i(\mathbf{k} + \mathbf{k}') \cdot \mathbf{r}} \\ &= -W_0^2 \int d^d \mathbf{r} \int \frac{d^d \mathbf{k} d^d \mathbf{k}'}{(2\pi)^{2d}} k_p k'_q [\mathcal{O}(t, \mathbf{k}), \mathcal{O}(0, \mathbf{k}')] e^{i(\mathbf{k} + \mathbf{k}') \cdot \mathbf{r}} \\ &= -W_0^2 \int \frac{d^d \mathbf{k} d^d \mathbf{k}'}{(2\pi)^d} \delta(\mathbf{k} + \mathbf{k}') k_p k'_q [\mathcal{O}(t, \mathbf{k}), \mathcal{O}(0, \mathbf{k}')] \\ &= W_0^2 \int \frac{d^d \mathbf{k}}{(2\pi)^d} k_p k_q [\mathcal{O}(t, \mathbf{k}), \mathcal{O}(0, -\mathbf{k})]. \end{aligned} \quad (62)$$

This gives us the retarded Green's function

$$\begin{aligned} \tilde{G}_{\dot{P}_p \dot{P}_q}^R(\omega, \mathbf{0}) &\equiv i \int_0^\infty dt e^{i\omega t} \tilde{F}_{\dot{P}_p \dot{P}_q}(t, \mathbf{0}, \mathbf{0}) \\ &= W_0^2 \int \frac{d^d \mathbf{k}}{(2\pi)^d} k_p k_q \tilde{G}_{\mathcal{O} \mathcal{O}}^R(\omega, \mathbf{k}), \end{aligned} \quad (63)$$

which we will simply write as $\tilde{G}_{\dot{P}_p \dot{P}_q}^R(\omega)$ to avoid cluttering of notations. Note that we have defined our retarded Green's function in presence of disorder as the one obtained after disorder averaging.

Due to the presence of the projection operator \mathcal{Q} in Eq. (48)], it is very hard to calculate the memory matrix M exactly. For this reason, we will resort to a useful approximation, which also shows the effectiveness of the approach. Since \dot{P}_p is linear in the disorder strength W_0 , the leading contribution to $M_{P_p P_q}$ is of order W_0^2 . Here, we

wish to keep the leading contribution only and, therefore, we approximate the full Liouville operator (after adding weak disorder) by simply the one without disorder, i.e., $L = [H^{(0)}, \circ]$. Additionally, we will calculate the ensemble-averages by using only $H^{(0)}$ instead of $H^{(0)} + H_{\text{imp}}$. Since \mathbf{P} is completely conserved for a clean system, $L P_p = 0$ and, consequently, $L \mathcal{Q} = L$. Hence, the memory matrix [cf. Eq. (48)] can be approximated by

$$\begin{aligned} M_{P_p P_q}(z) &\approx i \left(P_p \left| L \mathcal{Q} \frac{1}{z - \mathcal{Q} L \mathcal{Q}} \mathcal{Q} L \right| P_q \right) \\ &= i \left(P_p \left| L \mathcal{Q} \frac{1}{z - L \mathcal{Q}} L \right| P_q \right) \\ &= i \left(P_p \left| L \frac{1}{z - L \mathcal{Q}} L \right| P_q \right) \\ &= i \left(\dot{P}_p \left| \frac{1}{z - L} L \right| \dot{P}_q \right) = \tilde{\gamma}_{\dot{P}_p \dot{P}_q}(z), \end{aligned} \quad (64)$$

using Eq. (44). In the limit z going to zero, we define

$$\begin{aligned} M_{P_p P_q}(0) &\equiv \lim_{\omega \rightarrow 0} \frac{1}{i\omega} \left[\tilde{G}_{\dot{P}_p \dot{P}_q}^R(\omega) - \tilde{G}_{\dot{P}_p \dot{P}_q}^R(0) \right] \\ &= \frac{1}{i} \partial_\omega \tilde{G}_{\dot{P}_p \dot{P}_q}^R(\omega) \Big|_{\omega=0} = \lim_{\omega \rightarrow 0} \frac{\text{Im} \tilde{G}_{\dot{P}_p \dot{P}_q}^R(\omega)}{\omega}. \end{aligned} \quad (65)$$

The last equality follows from the fact that $\text{Re} \tilde{G}_{\dot{P}_p \dot{P}_q}^R(\omega)$ is an even function of ω , whereas $\text{Im} \tilde{G}_{\dot{P}_p \dot{P}_q}^R(\omega)$ is an odd function of ω [124].

In a time-reversal-invariant theory, in which momentum is the only almost-conserved observable, $N = 0$, and Eq. (46) gives us a diagonal component of the electrical conductivity tensor as

$$\sigma_{pp}(\omega, T) \equiv \frac{\chi_{J_p P_p}^2}{M_{P_p P_p}(\omega) - i\omega \chi_{P_p P_p}}. \quad (66)$$

Here, $\chi_{P_p P_q}$ is the momentum-momentum static susceptibility, and $\chi_{J_p J_q}$ is the current-momentum static susceptibility. This immediately tells us that the corresponding dc electrical conductivity is given by

$$\sigma_{pp}^{\text{dc}} \equiv \sigma_{pp}(0, T) = \frac{\chi_{J_p P_p}^2}{M_{P_p P_p}(0)}. \quad (67)$$

Electric and thermal transport generally couple together in charged quantum matter. Hence, we would want to compute not just the electrical conductivity, but a more general matrix of thermoelectric conductivity tensors. For this, we need to consider the heat current \mathbf{J}^Q , which naturally couples to a temperature gradient $\nabla_r T$ [110]. At the linear order, we have the generalized Ohm/Fourier law [71]

$$\begin{pmatrix} J_p \\ J_p^Q \end{pmatrix} = \sum_q \begin{pmatrix} \sigma_{pq} & \alpha_{pq} \\ T \alpha_{pq} & \bar{\kappa}_{pq} \end{pmatrix} \begin{pmatrix} E_q \\ -\partial_{r_q} T \end{pmatrix}, \quad (68)$$

following the notations of Ref. [131]. While the thermoelectric conductivity tensor α determines the Peltier, Seebeck, and Nernst effects, $\bar{\kappa}$ is the linear response coefficient between the heat current and the temperature gradient at

vanishing electric field. The latter applies to samples connected to conducting leads, allowing for a stationary current flow. In experiments, one often measures the components of the thermal conductivity tensor κ , which provide the coefficients between the heat current and temperature gradient at vanishing electric current (i.e., $\mathbf{J} = 0$), and are given by

$$\kappa = \bar{\kappa} - T \alpha \sigma^{-1} \alpha. \quad (69)$$

Finally, the Nernst response is defined as the electric field (\mathbf{E}_{ind}) induced by a thermal gradient, in the absence of an electric current, and is given in by the relation

$$\mathbf{E}_{\text{ind}} = -\vartheta \nabla_r T, \text{ where } \vartheta = -\sigma^{-1} \alpha. \quad (70)$$

From our discussions, we find that we need to specify a set of three tensors, viz. σ , α , and $\bar{\kappa}$, from which we can derive the remaining tensors listed above. In conjunction with Eq. (66), we have the relations

$$\begin{aligned} \bar{\kappa}_{pq}(\omega, T) &= \frac{1}{T} \Upsilon_{J_p^Q J_q^Q}(\omega), \\ \alpha_{pq}(\omega, T) &= \frac{1}{T} \Upsilon_{J_p J_q^Q}(\omega). \end{aligned} \quad (71)$$

Analogous to the electrical dc conductivity tensor, the diagonal components in the low-frequency limit are given by

$$\begin{aligned} \bar{\kappa}_{pp}^{\text{dc}} &= \frac{1}{T} \frac{\chi_{J_p^Q P_p}^2}{M_{P_p P_p}(0)}, \\ \alpha_{pp}^{\text{dc}}(T) &= \frac{1}{T} \chi_{J_p P_p} M_{P_p P_p}^{-1}(0) \chi_{P_p J_p^Q}. \end{aligned} \quad (72)$$

3. Generalized conductivity tensors in the presence of a weak magnetic field

We will now rederive the expressions for the conductivity tensors in the presence of a uniform magnetic field \mathbf{B} , with B denoting its magnitude [28, 58, 119, 120, 132]. We will focus on the regime where B is perturbatively small, such that the cyclotron frequency ω_c is a perturbatively small parameter as well, and follow the route of Ref. [58]. In this case, the time-reversal symmetry breaking matrix N is nonvanishing. We note that each component of M is first order within a perturbation theory — hence, it will suffice to consider only the B -dependent corrections to the M . This is because considering B -dependent corrections to the static susceptibility matrices will generate a higher-order correction. However, within the memory matrix formalism, any B -dependent correction to a parity-even component like $M_{P_p P_q}$ must be $\mathcal{O}(B^2)$. Consequently, the only matrix which may admit an $\mathcal{O}(B)$ correction is N . Therefore, we need compute the consequences of a nonzero B on N only.

For nonzero B , the zero-momentum component of the canonical momentum operator \mathcal{P}_B , which generates translations, no longer equivalent to the physical momentum operator. Instead, it is given by

$$\mathcal{P}^{(B)} = \mathbf{P} + \int d^d \mathbf{r} n_c \mathbf{A}_B, \quad (73)$$

where \mathbf{A}_B is a vector potential corresponding to the applied magnetic field \mathbf{B} . Although \mathbf{P} is gauge-invariant, the second term is not, since the form of \mathbf{A}_B depends on the choice of gauge. the effective Hamiltonian also needs to be modified as $H^{(0)} \rightarrow H^{(0)} + H_B$, where

$$H_B = - \int d^d \mathbf{r} \mathbf{J} \cdot \mathbf{A}_B. \quad (74)$$

For demonstration purposes, let us choose to consider a two-dimensional system (i.e., set $d = 2$). In order to evaluate \dot{P}_x , for example, a convenient gauge choice is $\mathbf{A}_B = -B y \hat{\mathbf{x}}$. This leads to

$$\begin{aligned} \dot{P}_x &= i \left[H^{(0)} + H_B, P_x \right] \\ &= i \left[H^{(0)} + H_B, \mathcal{P}_x^{(B)} + \frac{B}{2} \int d^2 \mathbf{r} n_c y \right] \\ &= i \left[H_B, \mathcal{P}_x^{(B)} \right] + B \int d^2 \mathbf{r} \dot{n}_c y + \mathcal{O}(B^2) \\ &= B \int d^2 \mathbf{r} (\partial_x J_x + \dot{n}_c) y \\ &= -B \int d^2 \mathbf{r} \partial_y J_y y = B \int d^2 \mathbf{r} J_y. \end{aligned} \quad (75)$$

A similar argument works for \dot{P}_y with the gauge choice $\mathbf{A}_B = B x \hat{\mathbf{y}}$. This leads to the expressions for the nonzero elements of N to be

$$N_{P_x P_y} = -N_{P_y P_x} = \chi_{P_x \dot{P}_y} = -B \chi_{J_x P_x}. \quad (76)$$

With these ingredients, we obtain

$$\begin{aligned} M(\omega) + N - i \omega \chi &= \begin{pmatrix} M_{P_x P_x} - i \omega \chi_{P_x P_x} & -B \chi_{J_x P_x} \\ B \chi_{J_x P_x} & M_{P_y P_y} - i \omega \chi_{P_y P_y} \end{pmatrix} + \mathcal{O}(B^2) \\ &= \begin{pmatrix} M_{P_x P_x} - i \omega \chi_{P_x P_x} & -B \chi_{J_x P_x} \\ B \chi_{J_x P_x} & M_{P_x P_x} - i \omega \chi_{P_x P_x} \end{pmatrix}. \end{aligned} \quad (77)$$

We can use this expression to evaluate the forms of the tensors σ , α , and $\bar{\kappa}$. In particular, the longitudinal and transverse components of the dc electrical conductivity tensor are given by

$$\begin{aligned} \sigma_{xx}^{\text{dc}} &= \frac{\chi_{J_x P_x}^2 M_{P_x P_x}}{M_{P_x P_x}^2 + B^2 \chi_{J_x P_x}^2} \text{ and} \\ \sigma_{xy} = -\sigma_{yx} &= \frac{B \chi_{J_x P_x}^3}{M_{P_x P_x}^2 + B^2 \chi_{J_x P_x}^2}, \end{aligned} \quad (78)$$

respectively.

C. Generic scaling arguments

Hyperscaling is the property that the free energy scales by its naive dimension [109, 133]. In a quantum system in d spatial dimensions, with dynamical critical exponent z , the free energy F has the scaling dimension

$$[F] = d + z. \quad (79)$$

Therefore, if hyperscaling is not violated, we should have the temperature-dependence

$$F \sim T^{d/z+1}. \quad (80)$$

The spatial components of the stress-energy tensor \mathcal{T}_{pq} have the same scaling dimension as the Lagrangian density and, hence,

$$[T_{zx}] = d + z. \quad (81)$$

Using the definition that

$$\eta \sim \tilde{G}_{\mathcal{T}_{pq}}^R(\omega), \quad (82)$$

where η is the shear viscosity, this implies that

$$\begin{aligned} [\eta] &= 2[T_{zx}] - z - [\text{Volume in energy-momentum space}] \\ &= 2(d+z) - z - d - z = d. \end{aligned} \quad (83)$$

This shows that η has the same scaling dimension as the entropy density s , which, by definition, is the derivative of the free energy with respect to T . Hence, the ratio η/s turns out to be dimensionless. If hyperscaling is not violated, Eq. (83) also implies the scaling form

$$\eta(\omega) \sim \omega^{d/z} \quad (84)$$

for optical viscosity (i.e., for $\omega \gg T$), and

$$\eta^{\text{dc}}(T) \sim T^{d/z} \quad (85)$$

for dc viscosity (i.e., for $T \gg \omega$).

In view of Eqs. (30) and (82), the scaling dimension for the conductivity tensor is [71]

$$\begin{aligned} [\sigma_{pq}] &= 2[\mathbf{J}] - z - [\text{Volume in energy-momentum space}] \\ &= 2(d+z-1) - z - d - z = d-2, \end{aligned} \quad (86)$$

which implies the scaling form

$$\sigma_{pq}(\omega) \sim \omega^{(d-2)/z} \quad (87)$$

for the optical conductivity. In scenarios when the hyperscaling is violated (see, for example, Ref. [17] for an NFL with a finite Fermi surface), the above scaling form is modified to

$$\sigma_{pq}(\omega) \sim \omega^{(d-2-\theta)/z}, \quad (88)$$

where θ represents a hyperscaling-violating exponent [134]. In Ref. [105], our results for the optical conductivity computed in the LAB phase shows hyperscaling violation.

III. TRANSPORT PROPERTIES OF THE LAB PHASE

As an example of an NFL arising at a Fermi point, we consider the 3d Luttinger semimetals [39–42, 89, 90, 92, 93, 105–107, 135–142], as discussed in the introduction. In this review, we will focus on isotropic but band-mass-asymmetric Luttinger semimetals, and show how various transport properties can be computed in the LAB phase by applying the techniques reviewed in the last section.

A. Minimal low-energy effective model

The effective low-energy continuum Hamiltonian, in the vicinity of the nodal point of an isotropic band-mass asymmetric Luttinger semimetal, is given by

$$\mathcal{H}_0 = \frac{|\mathbf{k}|^2}{2m'} - \frac{\frac{5}{4}k^2 - (\mathbf{k} \cdot \mathcal{J})^2}{2m}, \quad (89)$$

where \mathcal{J} represents the vector angular momentum operator in the spin-3/2 representation of the SO(3) group. Therefore, the Hamiltonian represents a system of noninteracting pseudospin-3/2 quasiparticles. The energy eigenvalues evaluate to

$$\epsilon_{\pm}(\mathbf{k}) = \frac{|\mathbf{k}|^2}{2m'} \pm \frac{|\mathbf{k}|^2}{2m}, \quad (90)$$

where the “+” and “-” signs refer to the conduction and valence bands, respectively, which are doubly-degenerate. Fig. 1(a) shows the schematics of the doubly-degenerate dispersion. The symbols m and m' represent the mass parameters of the quadratically dispersing bands. Since the term $\frac{|\mathbf{k}|^2}{2m'}$ multiplies an identity matrix, it causes the effective band masses of the conduction and valence bands to be asymmetric/unequal.

Following Refs. [40, 41, 89, 143], the Hamiltonian in Eq. (89) can be brought to the form

$$\mathcal{H}_0 = \sum_{a=1}^5 d_a(\mathbf{k}) \Gamma_a + \frac{|\mathbf{k}|^2}{2m'}, \quad (91)$$

where the set of five Γ_a -matrices forms a rank-four irreducible representation of the Euclidean Clifford algebra. Therefore, they obey the anticommutation relation $\{\Gamma_a, \Gamma_b\} = 2\delta_{ab}$. They can always be chosen such that three are real and two are imaginary [144].

The five $d_a(\mathbf{k})$ -functions are the real $\ell = 2$ spherical harmonics with the following structures [40, 41, 143]:

$$\begin{aligned} d_1(\mathbf{k}) &= \frac{\sqrt{3}k_y k_z}{2m}, & d_2(\mathbf{k}) &= \frac{\sqrt{3}k_x k_z}{2m}, & d_3(\mathbf{k}) &= \frac{\sqrt{3}k_x k_y}{2m} \\ d_4(\mathbf{k}) &= \frac{\sqrt{3}(k_x^2 - k_y^2)}{4m}, & d_5(\mathbf{k}) &= \frac{2k_z^2 - k_x^2 - k_y^2}{4m}. \end{aligned} \quad (92)$$

Henceforth, we will use the notation

$$\mathbf{d}_{\mathbf{k}} \equiv [d_1(\mathbf{k}), d_2(\mathbf{k}), d_3(\mathbf{k}), d_4(\mathbf{k}), d_5(\mathbf{k})] \quad (93)$$

to refer to the vector consisting of the five $d_a(\mathbf{k})$ -functions. Analogously, $\mathbf{\Gamma}$ will denote the vector whose components are the five Γ_a -matrices.

Adding the Coulomb interactions via a non-dynamical scalar boson field φ , the Euclidean action of the resulting interacting system can be straightforwardly written as

$$\begin{aligned} S_{\text{int}} &= \int d\tau d^3\mathbf{r} \left[\psi^\dagger(\tau, \mathbf{r}) \{ \partial_\tau + \mathcal{H}_0 + i e \varphi \} \psi(\tau, \mathbf{r}) \right. \\ &\quad \left. + \frac{c}{2} \{ \nabla \varphi(\tau, \mathbf{r}) \}^2 \right]. \end{aligned} \quad (94)$$

Here, ψ denotes the fermionic field, which is a four-component spinor, and c is a constant equal to $1/(4\pi)$.

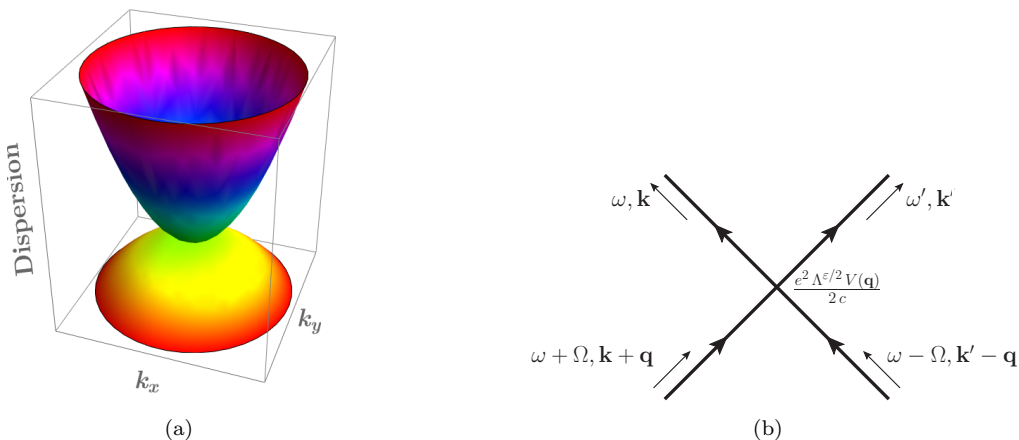


FIG. 1. (a) Schematics of the low-energy effective dispersion of an isotropic but band-mass-asymmetric Luttinger semimetal that harbours a doubly-degenerate quadratic band-touching at the Γ -point. (b) The four-fermion vertex arising due to Coulomb interactions.

We now extend the theory to a generic number of spatial dimensions d , to make it possible to apply dimensional

regularization. Finally, we integrate out φ to express the Coulomb interaction as an effective four-fermion interaction vertex, resulting in the form

$$\begin{aligned}
S &= \int \frac{d\tau d^d \mathbf{k}}{(2\pi)^d} \psi^\dagger(\tau, \mathbf{k}) (\partial_\tau + \mathcal{H}_0) \psi(\tau, \mathbf{k}) \\
&+ \frac{e^2 \Lambda^\varepsilon}{2c} \int \frac{d\tau d^d \mathbf{k} d^d \mathbf{k}' d^d \mathbf{q}}{(2\pi)^{3d}} V(\mathbf{q}) \psi^\dagger(\tau, \mathbf{k} + \mathbf{q}) \psi(\tau, \mathbf{k}) \psi^\dagger(\tau, \mathbf{k}' - \mathbf{q}) \psi(\tau, \mathbf{k}') \\
&= \int \frac{d\omega d^d \mathbf{k}}{(2\pi)^{d+1}} \tilde{\psi}^\dagger(\omega, \mathbf{k}) (-i\omega + \mathcal{H}_0) \tilde{\psi}(\omega, \mathbf{k}) \\
&+ \frac{e^2 \Lambda^{\varepsilon/2}}{2c} \int \frac{d\omega d\omega' d\Omega d^d \mathbf{q} d^d \mathbf{k} d^d \mathbf{k}'}{(2\pi)^{3(d+1)}} V(\mathbf{q}) \tilde{\psi}^\dagger(\omega, \mathbf{k}) \tilde{\psi}^\dagger(\omega', \mathbf{k}') \tilde{\psi}(\omega + \Omega, \mathbf{k} + \mathbf{q}) \tilde{\psi}(\omega' - \Omega, \mathbf{k}' - \mathbf{q}), \quad (95)
\end{aligned}$$

where $V(\mathbf{q}) = 1/|\mathbf{q}|^2$. In the momentum space, the Coulomb interaction vertex is given by $\frac{e^2 \Lambda^\varepsilon}{2c} V(|\mathbf{q}|)$, and $\tilde{\psi}_i^\dagger$ and $\tilde{\psi}$ represent Fourier-transformed fermionic fields. The four-fermion vertex is depicted schematically in Fig. 1(b). We have also scaled e^2/c by using the floating mass scale Λ (of the RG flow) so that its engineering dimension vanishes at $d = 4 - \varepsilon$. Here, we have determined the tree-level scaling dimensions of the fields and couplings by setting the scaling dimension of \mathbf{k} as $[\mathbf{k}] = 1$. Hence, the various engineering dimensions are given by: $[\tau] = -z = -2$ (where z is the dynamical critical exponent), $[1/m] = [1/m'] = z - 2$, and $[e^2] = 2z - d$ (before using the scaling factor Λ^ε).

The bare Green's function for each fermionic flavour, obtained from \mathcal{H}_0 , is given by

$$G_0(k_0, \mathbf{k}) = \frac{i k_0 - \frac{|\mathbf{k}|^2}{2m'} + \mathbf{d}_\mathbf{k} \cdot \boldsymbol{\Gamma}}{-\left(i k_0 - \frac{|\mathbf{k}|^2}{2m'}\right)^2 + |\mathbf{d}_\mathbf{k}|^2}, \quad (96)$$

where $|\mathbf{d}_\mathbf{k}|^2$ evaluates to $|\mathbf{k}|^4/(4m^2)$. From the one-loop fermionic self-energy, the upper critical dimension of the interacting system described by Eq. (95) turns out to

be $d_c = 4$. When we derive the RG flow equations of the model, a stable NFL fixed point in the infrared (which is the LAB fixed point) is found to exist for $d = 4 - \varepsilon$ (analogous to the Wilson-Fisher fixed point of the bosonic ϕ^4 -theory in $4 - \varepsilon$ dimensions [145]). As a result, we can extract the critical scalings of the system by a controlled approximation using an ε -expansion about d_c [37, 39]. At the LAB fixed point, the coupling constant e takes the value

$$e^{*2} = \frac{60 \pi^2 c \varepsilon}{19 m}. \quad (97)$$

The fixed point value of the dynamical critical exponent z is given by $z^* = 2 - 4\varepsilon/19$ [39]. It is to be noted that the results obtained using dimensional regularization can also be obtained by large- N methods.

Employing the Noether's theorem [146], the current (\mathbf{J}) and the momentum (\mathbf{P}) operators, associated with the invariance of the action of Eq. (95) under the global $U(1)$ symmetry and the continuous spatial translations, are given

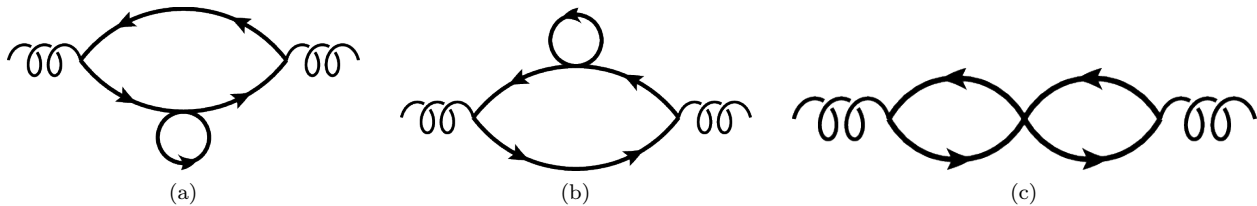


FIG. 2. Representation of the Feynman diagrams for the current-current correlator at two-loop order. Subfigures (a) and (b) denote the diagrams with fermionic self-energy insertions, while subfigure (c) represents the diagram with the insertion of a vertex correction.

by [105]

$$\begin{aligned}
 \mathbf{J}(q_0, \mathbf{q}) &= \sum_i \int \frac{dk_0 d^d \mathbf{k}}{(2\pi)^{d+1}} \tilde{\psi}_i^\dagger(k_0 + q_0, \mathbf{k} + \mathbf{q}) [\nabla_{\mathbf{k}} \mathbf{d}(\mathbf{k}) \cdot \mathbf{\Gamma}] \tilde{\psi}_i(k_0, \mathbf{k}), \\
 \mathbf{P}(q_0, \mathbf{q}) &= \sum_i \int \frac{dk_0 d^d \mathbf{k}}{(2\pi)^{d+1}} (\mathbf{k} + \mathbf{q}/2) \tilde{\psi}_i^\dagger(k_0 + q_0, \mathbf{k} + \mathbf{q}) \tilde{\psi}_i(k_0, \mathbf{k}).
 \end{aligned} \tag{98}$$

Analogously, the thermal current operator can be expressed as [106]

$$\mathbf{J}^Q(t, \mathbf{q}) = \frac{1}{2} \int \frac{d^d \mathbf{k}}{(2\pi)^d} \left[\partial_t \psi_i^\dagger(t, \mathbf{k} + \mathbf{q}) \left(\nabla_{\mathbf{k}} \mathbf{d} \cdot \mathbf{\Gamma} + \frac{\mathbf{k}}{m'} \right) \psi(t, \mathbf{k}) + \psi_i^\dagger(t, \mathbf{k} + \mathbf{q}) \left(\nabla_{\mathbf{k}} \mathbf{d} \cdot \mathbf{\Gamma} + \frac{\mathbf{k}}{m'} \right) \partial_t \psi(t, \mathbf{k}) \right], \tag{99}$$

where $\partial_t \psi \equiv i[\mathcal{H}_0, \psi]$.

B. Optical electrical conductivity

Using the Kubo formula derived in Sec. II A [cf. Eq. (82)], each longitudinal component of the isotropic optical conductivity tensor at $T = 0$ is equal to [105]

$$\sigma_{zz}(\omega, T) = - \frac{\langle J_z J_z \rangle(k_0)}{k_0} \Big|_{i k_0 \rightarrow \omega + i 0^+}, \tag{100}$$

with J_z is given by Eq. (98). Here, the symbol $\langle \dots \rangle$ denotes a correlator evaluated using the action in the Matsubara frequency space [in particular, using the second line of Eq. (95)]. By calculating the correlator $\langle J_z J_z \rangle$ in $d = 4 - \varepsilon$ upto two-loop order (cf. Fig. 2), we obtain [105]

$$\sigma_{zz}(\omega) \sim \omega^{1 - \frac{\varepsilon}{2} + \frac{5\varepsilon}{114}}, \tag{101}$$

This scaling dependence differs from the form $\omega^{(d-2)/z}$, which indicates hyperscaling violation, similar to the NFLs arising at hot-spots of a finite Fermi surface in a 2d fermion-boson system [147].

C. dc electrical conductivity

To find the dc electrical conductivity, we resort to the memory matrix formalism of Sec. II B, as we are then con-

sidering the limit $T \gg \omega$. We first calculate $\chi_{J_z P_z}$ and $M_{P_z P_z}(0)$ appearing in Eq. (67). For this calculation, we work directly in $d = 3$, as the memory matrix approach inherently takes care of the NFL behaviour of the system, without the need for a controlled expansion (e.g., by using small- ε or large- N). Since we are required to provide a mechanism of momentum relaxation via adding a weak disorder, it is not valid in the $T \rightarrow 0$ limit. This is because the impurity term in Eq. (57) is a relevant perturbation [40, 41] when we add it to the action described in Eq. (95). Consequently, the assumption of weak disorder is valid only in the $T \gg \omega$ limit, where the temperature plays the role of a cutoff in the RG flows (thus preventing the disorder strength from flowing to nonperturbative values), and the perturbative evaluation of the memory matrix to $\mathcal{O}(W_0^2)$ stands on firm ground.

While computing the momentum integrals, we are required to impose a ultraviolet (UV) cutoff Λ_0 at the outset, which is physical since there is a natural lattice cutoff for any solid state system. By taking into account the diagrams with self-energy feedback and vertex corrections (see Fig. 2), and evaluating the corresponding integrals numerically, we have obtained $\sigma_{zz}^{\text{dc}} \sim T^{n_\sigma}$, where $2 \lesssim n_\sigma \lesssim 4$ [105]. We note that this prediction compares well with the experimental data [148] for $(Y_{1-x}Pr_x)_2\text{Ir}_2\text{O}_7$, which predicts the same scaling for with the value $n \approx 2.98$ at zero doping (i.e., when the chemical potential cuts the nodal point).

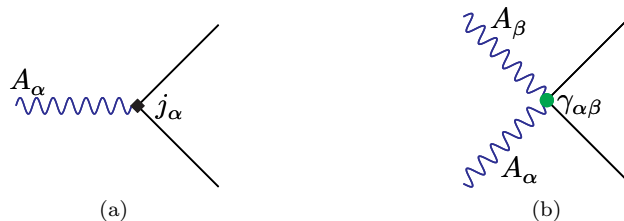


FIG. 3. Electron-photon coupling vertices for the Raman response. The blue curly lines represent the incident and scattered photons. (a) The first type of vertex represents coupling the electron's current to a single photon, and is denoted with a black square. (b) The second type of vertex represents coupling the electron's charge to two photons, and is denoted by a green dot.

D. Thermal and thermoelectric response

We apply the memory matrix formalism to calculate the thermal and thermoelectrical response, upto two-loop order, by taking into account Feynmann diagrams similar to those shown in Fig. 2. The final results are found to be [106] are captured by

$$\bar{\kappa}^{\text{dc}} \sim T^{-n_\kappa}, \text{ where } 0 \lesssim n_\kappa \lesssim 1, \quad (102)$$

$$\alpha^{\text{dc}} \sim T^{n_\alpha}, \text{ where } 1/2 \lesssim n_\alpha \lesssim 3/2. \quad (103)$$

For $T < 1$, although $\bar{\kappa}^{\text{dc}}$ is suppressed as a power-law as a function of T , α^{dc} can be reasonably high in the same regime. Since the experimentally relevant thermal conductivity is given by κ , we compute it using Eq. (69). The result shows that κ vanishes at leading order [106]. Consequently, in this system, the thermal conductivity at zero electric current could potentially be dominated by the phonon contribution, even below the Debye temperature.

Regarding the thermoelectric properties of the LAB phase, its efficiency is better captured in terms of either the Seebeck coefficient $\mathcal{S} = \alpha/\sigma_{dc}$, or the figure of merit $\mathcal{S}^2 \sigma^{\text{dc}} T/\kappa$. Analyzing their scaling forms, we have found that they can be quite high [106], which suggests that the Luttinger semimetals might be extremely useful for thermoelectric applications.

E. Raman response

Raman scattering is another fundamental tool that provides valuable information about the dynamics of the system [149–152]. A comprehensive review about this experimental technique can be found in Ref. [153]. Raman experiments involve the coupling of the electrons to an electromagnetic field representing the incoming and outgoing photons. This is incorporated by adding a gauge coupling via the Peierls substitution $\mathbf{k} \rightarrow \mathbf{k} + e\mathbf{A}/c$, where \mathbf{A} is the vector potential. In the resulting Hamiltonian, the terms depending on the vector potential are given by [107]

$$\mathcal{H}_{\mathbf{A}} = \frac{e}{c} A_\alpha j_p(\mathbf{k}) + \frac{e^2}{2c^2} A_p A_q \gamma_{pq}(\mathbf{k}), \quad (104)$$

where $j_p = \frac{k_p}{m'} + \partial_{k_p} d_a(\mathbf{k}) \Gamma_a$ represents the p^{th} -component of the current operator, and

$$\begin{aligned} \gamma_{xx} &= \frac{\Gamma_0}{m'} + \frac{\sqrt{3}\Gamma_4 - \Gamma_5}{2m}, & \gamma_{yy} &= \frac{\Gamma_0}{m'} - \frac{\sqrt{3}\Gamma_4 + \Gamma_5}{2m}, \\ \gamma_{zz} &= \frac{\Gamma_0}{m'} + \frac{\Gamma_5}{m}, & \gamma_{xy} = \gamma_{yx} &= \frac{\sqrt{3}\Gamma_3}{m}, \\ \gamma_{yz} = \gamma_{zy} &= \frac{\sqrt{3}\Gamma_1}{m}, & \gamma_{xz} = \gamma_{zx} &= \frac{\sqrt{3}\Gamma_2}{m}. \end{aligned} \quad (105)$$

We note that Eq. (104) gives rise to two types of electron-photon coupling vertices. While calculating the loop diagrams, we find that the contributing vertices can only be either (Γ_0, Γ_0) or (Γ_a, Γ_b) for $a, b \in \{1, \dots, 5\}$, since the remaining cross-terms turn out to vanish identically [107].

Quantizing the vector potential, one obtains

$$\mathbf{A}(\mathbf{k}) = \sqrt{\frac{c^2}{\omega_{\mathbf{k}} V}} \left(\hat{\mathbf{e}}_{\mathbf{k}} a_{-\mathbf{k}} + \hat{\mathbf{e}}_{\mathbf{k}}^* a_{\mathbf{k}}^\dagger \right), \quad (106)$$

where V is the volume. The operators $a_{\mathbf{q}}^\dagger$ and $a_{\mathbf{q}}$ are the creation and annihilation operators, respectively, of the photons with the dispersion relation $\omega_{\mathbf{k}} = c|\mathbf{k}|$, and having a polarization direction defined by $\hat{\mathbf{e}}_{\mathbf{k}}$.

The Raman scattering cross-section within the Born approximation is given by:

$$\frac{d^2\sigma}{d\Omega d\omega_{\text{in}}} \propto \sum_{F,I} \frac{\exp(-\beta E_I)}{Z} |\mathcal{M}_{FI}|^2 \delta(E_F + \omega_{\text{fi}} - E_I - \omega_{\text{in}}), \quad (107)$$

where I and F represent the initial and final states of the Luttinger semimetal, Z is the (canonical) partition function, and $\mathcal{M}_{FI} = \langle F | \mathcal{M} | I \rangle$, where \mathcal{M} is the effective light-scattering operator. The summation over F and I stands for a thermodynamic average over all possible initial and over final states of the system, possessing energies E_I and E_F , respectively, with the momentum vectors inside the solid angle element $d\Omega$. Moreover, $\omega = \omega_{\text{in}} - \omega_{\text{fi}}$ is the frequency and \mathbf{q} is the momentum transferred by the photons.

We define the operators $\rho_0 = \psi^\dagger \psi$ and $\rho_a = \psi^\dagger \Gamma_a \psi$, since their two-point correlators will contribute to the Raman response $|\mathcal{M}_{FI}|^2$. If we consider scattering in the visible range, a good approximation for the relevance of such a quantity is the zero momentum limit. Hence, we will focus on expressions for the correlators $\langle \rho_0 \rho_0 \rangle(k_0)$ and

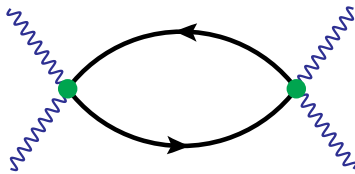


FIG. 4. Feynman diagram for the contribution to the Raman response at one-loop order.

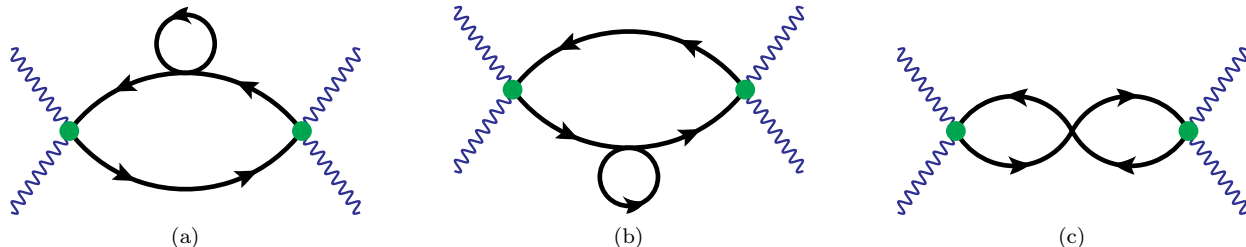


FIG. 5. Feynman diagrams for the contributions to the Raman response at two-loop order, with subfigures (a) and (b) representing the self-energy corrections, and subfigure (c) depicting the vertex correction.

$\langle \rho_a \rho_b \rangle(k_0)$ upto the two-loop order. The Feynman diagrams for computing $|\mathcal{M}_{FI}|^2$ involve vertices of two types, as depicted in Fig. 3. However, only diagrams consisting solely of green vertices involve non-resonant scatterings, while the others give rise to resonant and mixed scatterings which can be neglected in the low-energy limit [153]. Consequently, we consider here only the leading-order Feynman diagrams for $|\mathcal{M}_{FI}|^2$ contributed by the non-resonant scatterings.

In the $T = 0$ limit, we employ the ε -expansion at the NFL fixed point to evaluate the relevant correlators. Figs. 4 and 5 show the Feynman diagrams at the one-loop and two-loop orders, respectively. The final results come out to be [107]:

$$\langle \rho_a \rho_b \rangle(\omega) = 0, \quad \langle \rho_a \rho_b \rangle(\omega) \simeq -\frac{m^{2-\frac{\varepsilon}{2}} |\omega|^{1-\frac{\varepsilon}{2} + \frac{\varepsilon}{38}} \delta_{ab}}{10\pi} \left(\frac{m}{\Lambda}\right)^{\frac{\varepsilon}{38}}. \quad (108)$$

This shows that the Raman response in the LAB phase should scale as $|\omega|^{1-\varepsilon/2+\varepsilon/38} \stackrel{\varepsilon=1}{\equiv} |\omega|^{1/2+1/38}$, in the regime where $\omega \gg T$.

Next, we review our results illustrating the behavior obtained for the Raman response in the $T \gg \omega$ regime. For this part, analogous to the calculations for the generalized conductivity tensors, we use the memory matrix formalism. As explained in Se. II B, the existence of a nearly-conserved operator is essential for applying the memory matrix formalism, which we have taken to be the momentum so far. However, the momentum operator turns out to have no influence on the Raman response [122], because it has no overlap with the operators $\{\rho_a\}$. For this reason, we use here ρ_a itself for computing the Raman response, since it is also a nearly conserved operator in the presence of weak disorder. Therefore, we set $\mathcal{O} = \rho_a$ in Eq. (59), and the time evolution of ρ_a is given by $\dot{\rho}_a = i[\mathcal{H}_0 + H_{\text{imp}}, \rho_a]$.

The Raman response at $T > 0$ is defined as [121, 122]

$$D_{\text{Raman}}(\omega, T) = i\omega \tilde{\Upsilon}_{\rho_a \rho_b}(\omega), \quad (109)$$

which can be approximated as

$$D_{\text{Raman}}(\omega, T) \approx \chi_{\rho_a \rho_b} \frac{i\omega}{M_{\rho_b \rho_b}(\omega) - i\omega \chi_{\rho_b \rho_b}} \chi_{\rho_b \rho_a}. \quad (110)$$

In this case, the memory matrix has the components

$$M_{\rho_a \rho_b}(\omega) \approx \text{Im} \tilde{G}_{\rho_a \rho_b}^R(\omega, T)/\omega, \quad (111)$$

for small ω -values. For the LAB phase, the above expression reduces to

$$M_{\rho_a \rho_b}(\omega) = \frac{W_0^2}{\omega} \int \frac{d^3 \mathbf{k}}{(2\pi)^3} \text{Im} \tilde{\Pi}_{ab}^R(\omega, \mathbf{k}), \quad (112)$$

where

$$\begin{aligned} \tilde{\Pi}_{ab}^R(\omega, \mathbf{k}) &= \tilde{\Pi}_{ab}(k_0, \mathbf{k})|_{i k_0 \rightarrow \omega + i 0^+}, \text{ and} \\ \tilde{\Pi}_{ab}(k_0, \mathbf{k}) &= -T \sum_{q_0} \int \frac{d^3 \mathbf{q}}{(2\pi)^3} \text{Tr}[\Gamma_a G_0(q_0 + k_0, \mathbf{q} + \mathbf{k}) \Gamma_b G_0(q_0, \mathbf{q})]. \end{aligned} \quad (113)$$

At low frequencies and finite temperatures, the real part can be approximated by its $\omega \Rightarrow 0$ value, which vanishes as a power law of T [121]. Therefore, we focus on the imaginary part, which, using the fact that $\chi_{\rho_a \rho_b} \propto \delta_{ab}$, takes the form [107]

$$\begin{aligned} \text{Im} D_{\text{Raman}}(\omega, T) &= \frac{\omega M_{\rho_a \rho_a} \chi_{\rho_a \rho_a}^2}{\omega^2 \chi_{\rho_a \rho_a}^2 + M_{\rho_a \rho_a}^2} \equiv \frac{\omega \tilde{\Gamma} \chi_{\rho_a \rho_a}}{\omega^2 + \tilde{\Gamma}^2}, \\ \tilde{\Gamma} &= M_{\rho_a \rho_a} \chi_{\rho_a \rho_a}^{-1}. \end{aligned} \quad (114)$$

Fig. 6 shows a representative behaviour of $\text{Im} D_{\text{Raman}}(\omega, T)$. From the nature of the curves, we can clearly see that the Raman response in the LAB phase exhibits a quasi-elastic peak at $\omega \approx \omega_{\text{max}} \text{Re} M_{\rho_a \rho_a}(0)/\chi_{\rho_a \rho_a}$, with a peak-height equal to $\chi_{\rho_a \rho_a}/2$. The static susceptibility, to the leading order, can be fitted to the functional form of

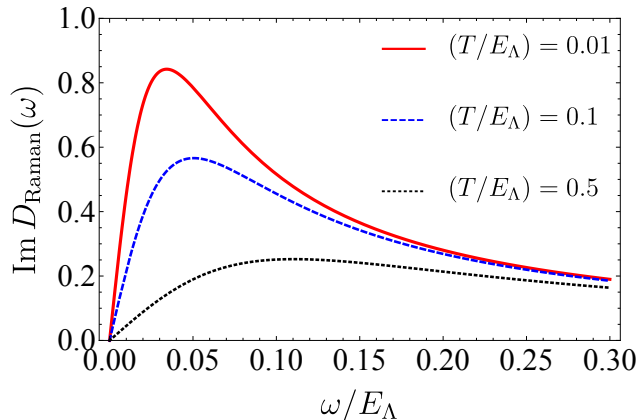


FIG. 6. Raman response as a function of frequency ω , for some representative values of the temperature T (as shown in the plot legends). The chosen parameter values for numerical evaluation are $\Lambda_0 = 10$, $m = 1$, $m' = 2$, $e^2/c = 1$, and $W_0 = 1$. The parameters T and ω are in units of $E_\Lambda = \Lambda_0^2/(2m)$, which is the ultraviolet energy cutoff used. E_Λ is of the order of the energy scale upto which the dispersion of the conduction and valence bands can be taken to be quadratic in the vicinity of the nodal point of the Luttinger semimetal.

$\chi_{\rho_a \rho_a} \simeq a_1 + a_2 T^{1/2} + a_3/T$, where a_1 , a_2 , and a_3 correspond to temperature-independent constants. Furthermore, $M_{\rho_a \rho_a}(0)$ is either T -independent, from a numerical point of view, or displays an extremely weak T -dependence, which is not observed within our numerical accuracy [107].

F. Shear viscosity and entropy density

In the hydrodynamic regime, shear viscosity η is one of the fundamental physical properties that describe the inherent characteristics of the system. In fluid mechanics, for example, η determines whether the hydrodynamic flow will be laminar or turbulent. In strongly correlated systems, η takes an even more important role — it expresses the degree of many-body quantum entanglement of the electronic phase. In a landmark paper by Kovtun, Son and Starinets [123], the authors have shown (by employing the AdS/CFT correspondence) that in strongly-interacting quantum field theories, the ratio of η with the entropy density s satisfies an inequality given by $(\eta/s) \geq \hbar/(4\pi k_B)$. If the universal lower bound is approximately saturated, the system is said to exhibit the “minimal-viscosity scenario”. Important examples of systems that satisfy the lower bound include quark-gluon plasma [123] generated in heavy-ion colliders, ultracold quantum gases trapped in optical lattices tuned to the unitary limit [154], and ultraclean graphene in the vicinity of the charge neutrality point [155]. Here, we review our results for η and s for the LAB phase.

Using the Kubo formula [156, 157], the isotropic optical shear viscosity in the $T = 0$ limit is given by

$$\begin{aligned} \eta(\omega) &= \lim_{\mathbf{q} \rightarrow 0} \frac{\langle \mathcal{T}_{xy} \mathcal{T}_{xy} \rangle(\omega, \mathbf{q})}{\omega} \\ &= \lim_{\mathbf{q} \rightarrow 0} \frac{\langle \mathcal{T}_{yz} \mathcal{T}_{yz} \rangle(\omega, \mathbf{q})}{\omega} \\ &= \lim_{\mathbf{q} \rightarrow 0} \frac{\langle \mathcal{T}_{zx} \mathcal{T}_{zx} \rangle(\omega, \mathbf{q})}{\omega}, \end{aligned} \quad (115)$$

where $\mathcal{T}_{\mu\nu}$ is the stress tensor. The variables μ and ν span

over the Matsubara frequency and the spatial components. For the LAB phase, the stress tensor takes the form

$$\begin{aligned} \mathcal{T}_{\mu\nu}(q_0, \mathbf{q}) &= \int \frac{dk_0 d^3\mathbf{k}}{(2\pi)^4} (k_\nu + q_\nu/2) \tilde{\psi}^\dagger(k_0 + q_0, \mathbf{k} + \mathbf{q}) \\ &\quad \times [\partial_{k^\mu}(\mathbf{d}_\mathbf{k} \cdot \boldsymbol{\Gamma})] \tilde{\psi}(k_0, \mathbf{k}). \end{aligned} \quad (116)$$

Evaluating the above expression using the fixed-point action, the optical viscosity is found to scale as [107]

$$\eta(\omega) \sim \omega^{2-\frac{\epsilon}{2}-\frac{367\epsilon}{2736}}. \quad (117)$$

Comparing with Eq. (84), we find that there is a small hyperscaling violation proportional to ϵ .

Using the memory matrix formalism, the temperature-dependent isotropic shear viscosity is given by [107]

$$\eta(\omega, T) = \chi_{\mathcal{T}_{pq} \mathcal{T}_{pq}} \left[\frac{1}{M_{\mathcal{T}_{pq} \mathcal{T}_{pq}} - i\omega \chi_{\mathcal{T}_{\mu\nu} \mathcal{T}_{pq}}} \right] \chi_{\mathcal{T}_{pq} \mathcal{T}_{pq}}, \quad (118)$$

We point out that, here, we have used the fact that the stress tensor turns out to be another nearly-conserved operator for the LAB phase in the limit of weak disorder [107].

In the dc limit, we obtain

$$\eta^{\text{dc}}(T) = \chi_{\mathcal{T}_{zx} \mathcal{T}_{zx}}^2 / M_{\mathcal{T}_{zx} \mathcal{T}_{zx}}. \quad (119)$$

In Ref. [107], we have evaluated the right-hand-side to get the result

$$\eta^{\text{dc}} \sim T^\lambda, \quad (120)$$

where λ turns out to be a non-universal exponent lying within the range $0 < \lambda < 1$.

The next step is to calculate the free energy at $T > 0$. Since the bosons have no dynamics, the contributions to this quantity come only from the free fermions and the perturbative corrections due to the Coulomb interactions [107]. We compute the latter by using the ϵ -expansion about $d_c = 4$. The contribution from the free fermions

is given by $\Delta F^{(0)} = F^{(0)} - F^{(0)}(0)$, where

$$\Delta F^{(0)} = -2 \int \frac{d^d \mathbf{k}}{(2\pi)^d} \left[T \sum_{l=\pm} \ln \left(1 + e^{-\frac{l|\mathbf{k}|^2}{2mT}} \right) - \frac{|\mathbf{k}|^2}{2m} \right], \quad (121)$$

where we must subtract the contribution from the T -independent ground state energy, and include a factor of 2 to account for the double-degeneracy of the bands. This final result takes the form [107]

$$\Delta F^{(0)} \simeq -\frac{\bar{\eta}(3) (mT)^{3-\frac{\epsilon}{2}}}{\pi^2 m} - \frac{3\zeta(3) (mT)^{3-\frac{\epsilon}{2}}}{4\pi^2 m}, \quad (122)$$

with $\bar{\eta}(u) = \frac{\int_0^\infty dt t^{u-2} \ln(1+e^{-t})}{\Gamma(u-1)}$ symbolizing the Dirichlet eta function, and we have set $\epsilon = 0$ in the numerical prefactors of the scaling arguments. The lowest-order correction in the free energy due to the Coulomb interaction reads [107]

$$F_{\text{int}} = \frac{e^2 \Lambda^\epsilon T^2}{c} \times \sum_{\Omega_n, \omega_{n'}} \int \frac{d^d \mathbf{q} d^d \mathbf{k}}{(2\pi)^{2d}} \frac{\text{Tr} [G(\omega_{n'} + \Omega_n, \mathbf{k} + \mathbf{q}) G(\omega_{n'}, \mathbf{k})]}{|\mathbf{q}|^2}, \quad (123)$$

where $\omega_{n'}$ and Ω_n represent the fermionic and bosonic Matsubara frequencies, respectively. Setting $d = 4 - \epsilon$, we need to isolate the contributions due to poles in the parameter ϵ . To lowest order in ϵ , these poles are obtained by evaluating one Matsubara frequency sum at $T > 0$ exactly, and the other one as an integral in the limit of $T \rightarrow 0$. Employing these steps, we get the final scaling form of the free energy as [107]

$$F \simeq -\frac{3\zeta(3) m^{2-\frac{\epsilon}{2}} T^{3-\frac{\epsilon}{2}-\frac{4\epsilon}{19}}}{4\pi^2} \left(\frac{\Lambda^2}{m} \right)^{\frac{4\epsilon}{19}}. \quad (124)$$

Extrapolating our results to the physical scenario of $d = 3$, we find that the free energy scales as

$$F(T) \sim T^{3-\frac{5}{2}-\frac{4\epsilon}{19}} \stackrel{\epsilon=1}{=} T^{\frac{5}{2}-\frac{4}{19}}. \quad (125)$$

This implies that the specific heat scales as

$$C(T) \sim T^{2-\frac{\epsilon}{2}-\frac{4\epsilon}{19}} \stackrel{\epsilon=1}{=} T^{\frac{3}{2}-\frac{4}{19}}. \quad (126)$$

Comparing with Eq. (80), and taking into account the fixed point value $z^* = 2 - \frac{4\epsilon}{19}$ for the dynamical critical exponent, we find that there is a hyperscaling violation, which is proportional to ϵ .

Using the fact that the entropy density is the derivative of the free energy with respect to the temperature, we get $s \sim T^{2-\frac{5}{2}-\frac{4\epsilon}{19}}$. Setting $d = 3$ (i.e., $\epsilon = 1$), this leads to

$$s \sim T^{2-\frac{27}{38}}. \quad (127)$$

Therefore,

$$\left(\frac{\eta^{\text{dc}}}{s} \right) \sim T^{\lambda-\frac{49}{38}}, \quad (128)$$

which indicates that η/s always tends to diverge at low temperatures, rather than saturating to a constant universal value. This divergent behavior bears some resemblances to the result found in the finite Fermi surface NFL arising at the Ising-nematic critical point [33]. In that particular scenario, the divergence emerges due to the violation of the hyperscaling property, whose origin can be related to the presence of a finite sharply-defined Fermi surface. We would like to point out that this divergent behavior of η/s , as a function of T , contrasts with the results obtained in Refs. [139, 158] which employed a quantum Boltzmann equation method.

IV. DISCUSSION AND OUTLOOK

In this review, we have examined the recent progress in constructing non-quasiparticle transport theories, which can be applied to various NFL phases. In particular, we have identified the Kubo formalism and the memory matrix approach as two useful frameworks to extract the transport properties. As an application of these two methods, we have demonstrated the computation of generalized conductivity tensors, Raman response, free energy, viscosity, and entropy density. In the so-called LAB phase of the Luttinger semimetals acted upon by unscreened Coulomb interactions. We have discussed the history and phenomenology of identifying the materials harbouring the LAB phase.

Overall, the investigation of NFL phases arising in nodal-point semimetals has seen great progress over the last decade. From a more theoretical standpoint, some future directions worthy of investigations are as follows:

1. The effect of phonons as a relaxation mechanism as a function in the finite-temperature transport properties is a very important aspect. As we have seen in our discussions for the LAB phase, phonons are expected to be relevant for some of the response characteristics. We would like to point out that this is in accord with the results reported in recent experimental works [159].
2. Finding a way to go beyond the weak disorder approximation usually used in the memory matrix formalism, when we want to slowly relax one of the conserved charges. One way to do so might be to follow in the footsteps of the SYK-Yukawa models [64–66, 68]), where an exact treatment of the effects of disorder have been achieved in the large- N limit.
3. The calculation of other fundamental magnetotransport coefficients like the planar Hall and planar thermal Hall effects [160–164], Nernst response [47, 165, 166], Magnus Hall effect [167–169], to name a few.
4. Computation of many-body quantum chaos parameters, such as the Lyapunov exponent λ_L and the “butterfly-effect” velocity v_B , by using the out-of-time-order correlators (OTOCs) [170], for example. Although these quantities are not experimentally measured, it was proposed in Refs. [171, 172] that they are related to important physical quantities such as the charge and energy diffusivities. The inverse of

the Lyapunov exponent represents the time in which the quantum information, associated with a local perturbation, gets “scrambled” into non-local degrees of freedom. On the other hand, v_B refers to the speed at which the effects of such a perturbation propagate in the system. Recently, Maldacena *et al.* [173] has shown that the Lyapunov time, $\tau_L \equiv 1/\lambda_L$, satisfies the inequality $\tau_L \geq \hbar/(2\pi k_B T)$. The Lyapunov time saturates to the universal lower bound of the inequality in scenarios like the SYK model [174], and if the corresponding quantum field theory is holographically dual to a black hole [175] and also .

On the experimental front, although some recent explorations [84, 159, 176, 177]) have found smoking-gun signatures that might turn out to be precursors to the physics of the LAB state, there is still no unambiguous evidence for the NFL phase appearing at the nodal point. More precise experiments are needed in this direction. Apart from the predictions for several transport signatures that we have reviewed here, other complementary characteristics, amenable to experimental measurements, will provide

important information about these systems. One important tool might be to apply the angle-resolved photoemission spectroscopy (ARPES) technique [178], that measures the single-particle lifetime for the low-energy excitations in the system. In such an experiment, a strong departure from the Fermi liquid behavior should be detected if the NFL phase can be accessed. Another promising experimental technique is the momentum-resolved electron energy loss spectroscopy (M-EELS) [179–181], that probes the dynamic charge response resolved in momentum.

ACKNOWLEDGMENTS

H.F. acknowledges funding obtained from the Conselho Nacional de Desenvolvimento Científico e Tecnológico (CNPq) under grant numbers 311428/2021-5 and 404274/2023-4. IM’s research leading to these results has received funding from the European Union’s Horizon 2020 research and innovation programme under the Marie Skłodowska-Curie grant agreement number 754340.

-
- [1] C. Nayak and F. Wilczek, Renormalization group approach to low temperature properties of a non-Fermi liquid metal, *Nuclear Physics B* **430**, 534 (1994).
 - [2] C. Nayak and F. Wilczek, Non-Fermi liquid fixed point in $2 + 1$ dimensions, *Nuclear Physics B* **417**, 359 (1994).
 - [3] M. J. Lawler, D. G. Barci, V. Fernández, E. Fradkin, and L. Oxman, Nonperturbative behavior of the quantum phase transition to a nematic Fermi fluid, *Phys. Rev. B* **73**, 085101 (2006).
 - [4] D. F. Mross, J. McGreevy, H. Liu, and T. Senthil, Controlled expansion for certain non-Fermi-liquid metals, *Phys. Rev. B* **82**, 045121 (2010).
 - [5] H.-C. Jiang, M. S. Block, R. V. Mishmash, J. R. Garrison, D. N. Sheng, O. I. Motrunich, and M. P. A. Fisher, Non-Fermi-liquid d-wave metal phase of strongly interacting electrons, *Nature (London)* **493**, 39 (2013).
 - [6] M. A. Metlitski and S. Sachdev, Quantum phase transitions of metals in two spatial dimensions. I. Ising-nematic order, *Phys. Rev. B* **82**, 075127 (2010).
 - [7] M. A. Metlitski and S. Sachdev, Quantum phase transitions of metals in two spatial dimensions. II. Spin density wave order, *Phys. Rev. B* **82**, 075128 (2010).
 - [8] S. B. Chung, I. Mandal, S. Raghu, and S. Chakravarty, Higher angular momentum pairing from transverse gauge interactions, *Phys. Rev. B* **88**, 045127 (2013).
 - [9] Z. Wang, I. Mandal, S. B. Chung, and S. Chakravarty, Pairing in half-filled Landau level, *Annals of Physics* **351**, 727 (2014).
 - [10] S. Sur and S.-S. Lee, Chiral non-Fermi liquids, *Phys. Rev. B* **90**, 045121 (2014).
 - [11] D. Dalidovich and S.-S. Lee, Perturbative non-Fermi liquids from dimensional regularization, *Phys. Rev. B* **88**, 245106 (2013).
 - [12] S. Sur and S.-S. Lee, Quasilocal strange metal, *Phys. Rev. B* **91**, 125136 (2015).
 - [13] I. Mandal and S.-S. Lee, Ultraviolet/infrared mixing in non-Fermi liquids, *Phys. Rev. B* **92**, 035141 (2015).
 - [14] I. Mandal, UV/IR mixing in non-Fermi liquids: Higher-loop corrections in different energy ranges, *Eur. Phys. J. B* **89**, 278 (2016).
 - [15] V. S. de Carvalho, T. Kloss, X. Montiel, H. Freire, and C. Pépin, Strong competition between Θ_{II} -loop-current order and d-wave charge order along the diagonal direction in a two-dimensional hot spot model, *Phys. Rev. B* **92**, 075123 (2015).
 - [16] V. S. de Carvalho, C. Pépin, and H. Freire, Coexistence of Θ_{II} -loop-current order with checkerboard d-wave CDW/PDW order in a hot-spot model for cuprate superconductors, *Phys. Rev. B* **93**, 115144 (2016).
 - [17] A. Eberlein, I. Mandal, and S. Sachdev, Hyperscaling violation at the Ising-nematic quantum critical point in two-dimensional metals, *Phys. Rev. B* **94**, 045133 (2016).
 - [18] I. Mandal, Superconducting instability in non-Fermi liquids, *Phys. Rev. B* **94**, 115138 (2016).
 - [19] I. Mandal, Scaling behaviour and superconducting instability in anisotropic non-Fermi liquids, *Annals of Physics* **376**, 89 (2017).
 - [20] S.-S. Lee, Recent developments in non-Fermi liquid theory, *Annual Review of Condensed Matter Physics* **9**, 227 (2018).
 - [21] D. Pimenov, I. Mandal, F. Piazza, and M. Punk, Non-Fermi liquid at the FFLO quantum critical point, *Phys. Rev. B* **98**, 024510 (2018).
 - [22] I. Mandal, Critical Fermi surfaces in generic dimensions arising from transverse gauge field interactions, *Phys. Rev. Research* **2**, 043277 (2020).
 - [23] I. Mandal, Stable non-Fermi liquid fixed point at the onset of incommensurate $2k_F$ charge density wave order, arXiv preprint (2024), [arXiv:2403.02322 \[cond-mat.str-el\]](https://arxiv.org/abs/2403.02322).
 - [24] D. Chowdhury, A. Georges, O. Parcollet, and S. Sachdev, Sachdev-Ye-Kitaev models and beyond: Window into non-Fermi liquids, *Reviews of Modern Physics* **94** (2022).
 - [25] S. Ono, S. Komiyama, and Y. Ando, Strong charge fluctuations manifested in the high-temperature hall coefficient of high- T_c cuprates, *Phys. Rev. B* **75**, 024515 (2007).
 - [26] A. Legros, S. Benhabib, W. Tabis, F. Laliberté, M. Dion, M. Lizaïre, B. Vignolle, D. Vignolles, H. Raffy, Z. Z. Li, P. Auban-Senzier, N. Doiron-Leyraud, P. Fournier, D. Col-

- son, L. Taillefer, and C. Proust, Universal T-linear resistivity and Planckian dissipation in overdoped cuprates, *Nature Physics* **15**, 142 (2018).
- [27] J. Ayres, M. Berben, M. Čulo, Y.-T. Hsu, E. van Heumen, Y. Huang, J. Zaanen, T. Kondo, T. Takeuchi, J. R. Cooper, C. Putzke, S. Friedemann, A. Carrington, and N. E. Hussey, Incoherent transport across the strange-metal regime of overdoped cuprates, *Nature* **595**, 661 (2021).
- [28] I. M. Hayes, R. D. McDonald, N. P. Breznay, T. Helm, P. J. W. Moll, M. Wartenbe, A. Shekhter, and J. G. Analytis, Scaling between magnetic field and temperature in the high-temperature superconductor $\text{BaFe}_2(\text{As}_{1-x}\text{P}_x)_2$, *Nature Physics* **12**, 916 (2016).
- [29] Y. Nakajima, K. Izawa, Y. Matsuda, K. Behnia, H. Kontani, M. Hedo, Y. Uwatoko, T. Matsumoto, H. Shishido, R. Settai, and Y. Onuki, Evolution of Hall coefficient in two-dimensional heavy fermion CeCoIn_5 , *Journal of the Physical Society of Japan* **75**, 023705 (2006).
- [30] Y. Cao, D. Chowdhury, D. Rodan-Legrain, O. Rubies-Bigorda, K. Watanabe, T. Taniguchi, T. Senthil, and P. Jarillo-Herrero, Strange metal in magic-angle graphene with near Planckian dissipation, *Physical Review Letters* **124** (2020).
- [31] I. Mandal and R. M. Fernandes, Valley-polarized nematic order in twisted moiré systems: In-plane orbital magnetism and crossover from non-Fermi liquid to Fermi liquid, *Phys. Rev. B* **107**, 125142 (2023).
- [32] A. A. Patel, P. Strack, and S. Sachdev, Hyperscaling at the spin density wave quantum critical point in two-dimensional metals, *Phys. Rev. B* **92**, 165105 (2015).
- [33] A. Eberlein, A. A. Patel, and S. Sachdev, Shear viscosity at the Ising-nematic quantum critical point in two-dimensional metals, *Phys. Rev. B* **95**, 075127 (2017).
- [34] M. A. Metlitski, D. F. Mross, S. Sachdev, and T. Senthil, Cooper pairing in non-Fermi liquids, *Phys. Rev. B* **91**, 115111 (2015).
- [35] S. Chakravarty, R. E. Norton, and O. F. Syljuåsen, Transverse gauge interactions and the vanquished Fermi liquid, *Phys. Rev. Lett.* **74**, 1423 (1995).
- [36] T. Senthil, Theory of a continuous Mott transition in two dimensions, *Phys. Rev. B* **78**, 045109 (2008).
- [37] A. A. Abrikosov, Calculation of critical indices for zero-gap semiconductors, *Soviet Journal of Experimental and Theoretical Physics* **39**, 709 (1974).
- [38] A. A. Abrikosov and S. D. Beneslavskii, Possible existence of substances intermediate between metals and dielectrics, in *30 Years of the Landau Institute - Selected Papers* (1996) pp. 64–73.
- [39] E.-G. Moon, C. Xu, Y. B. Kim, and L. Balents, Non-Fermi-liquid and topological states with strong spin-orbit coupling, *Phys. Rev. Lett.* **111**, 206401 (2013).
- [40] R. M. Nandkishore and S. A. Parameswaran, Disorder-driven destruction of a non-Fermi liquid semimetal studied by renormalization group analysis, *Phys. Rev. B* **95**, 205106 (2017).
- [41] I. Mandal and R. M. Nandkishore, Interplay of Coulomb interactions and disorder in three-dimensional quadratic band crossings without time-reversal symmetry and with unequal masses for conduction and valence bands, *Phys. Rev. B* **97**, 125121 (2018).
- [42] I. Mandal, Fate of superconductivity in three-dimensional disordered Luttinger semimetals, *Annals of Physics* **392**, 179 (2018).
- [43] B. Roy, M. P. Kennett, K. Yang, and V. Juričić, From birefringent electrons to a marginal or non-Fermi liquid of relativistic spin-1/2 fermions: An emergent superuniversity, *Phys. Rev. Lett.* **121**, 157602 (2018).
- [44] I. Mandal, Robust marginal Fermi liquid in birefringent semimetals, *Physics Letters A* **418**, 127707 (2021).
- [45] R. Kubo, A general expression for the conductivity tensor, *Canadian Journal of Physics* **34**, 1274 (1956).
- [46] R. Kubo, Statistical-mechanical theory of irreversible processes. I. General theory and simple applications to magnetic and conduction problems, *Journal of the Physical Society of Japan* **12**, 570 (1957).
- [47] I. Mandal and K. Saha, Thermoelectric response in nodal-point semimetals, arXiv e-prints (2023), arXiv:2309.10763 [cond-mat.mes-hall].
- [48] R. E. Prange and L. P. Kadanoff, Transport theory for electron-phonon interactions in metals, *Phys. Rev.* **134**, A566 (1964).
- [49] Y. B. Kim, P. A. Lee, and X.-G. Wen, Quantum Boltzmann equation of composite fermions interacting with a gauge field, *Phys. Rev. B* **52**, 17275 (1995).
- [50] I. Mandal, Zero sound and plasmon modes for non-Fermi liquids, *Physics Letters A* **447**, 128292 (2022).
- [51] K. R. Islam and I. Mandal, Generic deformation channels for critical Fermi surfaces in the collisionless regime, *Annals of Physics* **457**, 169409 (2023).
- [52] H. Mori, Transport, collective motion, and Brownian motion, *Progress of Theoretical Physics* **33**, 423 (1965).
- [53] H. Mori, A continued-fraction representation of the time-correlation functions, *Progress of Theoretical Physics* **34**, 399 (1965).
- [54] R. Zwanzig, Ensemble method in the theory of irreversibility, *The Journal of Chemical Physics* **33**, 1338 (1960), https://pubs.aip.org/aip/jcp/article-pdf/33/5/1338/18820045/1338_1_online.pdf.
- [55] R. Zwanzig, Memory effects in irreversible thermodynamics, *Phys. Rev.* **124**, 983 (1961).
- [56] W. Götze and P. Wölfle, Homogeneous dynamical conductivity of simple metals, *Phys. Rev. B* **6**, 1226 (1972).
- [57] D. Forster, *Hydrodynamic fluctuations, broken symmetry, and correlation functions*, Advanced Books Classics (CRC Press, 1995).
- [58] A. Lucas and S. Sachdev, Memory matrix theory of magnetotransport in strange metals, *Phys. Rev. B* **91**, 195122 (2015).
- [59] B. R. Green, *Memory Function Formalism for the Electrical Conductivity of Periodic Systems*, Ph.D. thesis, The Pennsylvania State University (2022).
- [60] S. Sachdev, What can gauge-gravity duality teach us about condensed matter physics?, *Annual Review of Condensed Matter Physics* **3**, 9–33 (2012).
- [61] S. A. Hartnoll, Lectures on holographic methods for condensed matter physics, *Classical and Quantum Gravity* **26**, 224002 (2009).
- [62] S. Sachdev and J. Ye, Gapless spin-fluid ground state in a random quantum Heisenberg magnet, *Phys. Rev. Lett.* **70**, 3339 (1993).
- [63] A. Kitaev, A simple model of quantum holography, *Talks at KITP, April 7 and May 27* (2015).
- [64] I. Esterlis and J. Schmalion, Cooper pairing of incoherent electrons: An electron-phonon version of the Sachdev-Ye-Kitaev model, *Phys. Rev. B* **100**, 115132 (2019).
- [65] Y. Wang, Solvable strong-coupling quantum-dot model with a non-Fermi-liquid pairing transition, *Phys. Rev. Lett.* **124**, 017002 (2020).
- [66] A. A. Patel and S. Sachdev, Critical strange metal from fluctuating gauge fields in a solvable random model, *Phys. Rev. B* **98**, 125134 (2018).
- [67] A. Halder, P. Halder, S. Bera, I. Mandal, and S. Banerjee, Quench, thermalization, and residual entropy across

- a non-Fermi liquid to Fermi liquid transition, *Phys. Rev. Res.* **2**, 013307 (2020).
- [68] E. E. Aldape, T. Cookmeyer, A. A. Patel, and E. Altman, Solvable theory of a strange metal at the breakdown of a heavy Fermi liquid, *Phys. Rev. B* **105**, 235111 (2022).
- [69] A. A. Patel, H. Guo, I. Esterlis, and S. Sachdev, Universal theory of strange metals from spatially random interactions, *Science* **381**, 790 (2023).
- [70] J. Zaanen, Y. Liu, Y.-W. Sun, and K. Schalm, *Holographic Duality in Condensed Matter Physics* (Cambridge University Press, Cambridge, 2015).
- [71] S. A. Hartnoll, A. Lucas, and S. Sachdev, Holographic quantum matter, *arXiv e-prints*, arXiv:1612.07324 (2016), arXiv:1612.07324 [hep-th].
- [72] P. W. Phillips, N. E. Hussey, and P. Abbamonte, Stranger than metals, *Science* **377**, eabh4273 (2022).
- [73] D. V. Else, R. Thorngren, and T. Senthil, Non-Fermi liquids as ersatz Fermi liquids: General constraints on compressible metals, *Phys. Rev. X* **11**, 021005 (2021).
- [74] C. M. Varma, P. B. Littlewood, S. Schmitt-Rink, E. Abrahams, and A. E. Ruckenstein, Phenomenology of the normal state of Cu-O high-temperature superconductors, *Phys. Rev. Lett.* **63**, 1996 (1989).
- [75] R. Mahajan, M. Barkeshli, and S. A. Hartnoll, Non-Fermi liquids and the Wiedemann-Franz law, *Phys. Rev. B* **88**, 125107 (2013).
- [76] A. A. Patel and S. Sachdev, dc resistivity at the onset of spin density wave order in two-dimensional metals, *Phys. Rev. B* **90**, 165146 (2014).
- [77] L. E. Vieira, V. S. de Carvalho, and H. Freire, DC resistivity near a nematic quantum critical point: Effects of weak disorder and acoustic phonons, *Annals of Physics* **419**, 168230 (2020).
- [78] A. Banerjee, M. Grandadam, H. Freire, and C. Pépin, Strange metal from incoherent bosons, *Phys. Rev. B* **104**, 054513 (2021).
- [79] C. Pépin and H. Freire, Charge order and emergent symmetries in cuprate superconductors, *Annals of Physics* **456**, 169233 (2023).
- [80] E. Pangburn, A. Banerjee, H. Freire, and C. Pépin, Incoherent transport in a model for the strange metal phase: Memory-matrix formalism, *Phys. Rev. B* **107**, 245109 (2023).
- [81] E. Berg, S. Lederer, Y. Schattner, and S. Trebst, Monte carlo studies of quantum critical metals, *Annual Review of Condensed Matter Physics* **10**, 63 (2019).
- [82] Z. H. Liu, G. Pan, X. Y. Xu, K. Sun, and Z. Y. Meng, Itinerant quantum critical point with fermion pockets and hotspots, *Proceedings of the National Academy of Sciences* **116**, 16760 (2019).
- [83] R. M. P. Teixeira, C. Pépin, and H. Freire, Strange metallicity in an antiferromagnetic quantum critical model: A sign-problem-free quantum Monte Carlo study, *Phys. Rev. B* **108**, 085131 (2023).
- [84] T. Kondo, M. Nakayama, R. Chen, J. J. Ishikawa, E.-G. Moon, T. Yamamoto, Y. Ota, W. Malaeb, H. Kanai, Y. Nakashima, and et al., Quadratic Fermi node in a 3D strongly correlated semimetal, *Nature Communications* **6** (2015).
- [85] N. P. Butch, P. Syers, K. Kirshenbaum, A. P. Hope, and J. Paglione, Superconductivity in the topological semimetal YPtBi, *Phys. Rev. B* **84**, 220504 (2011).
- [86] F. F. Tafti, T. Fujii, A. Juneau-Fecteau, S. René de Cotret, N. Doiron-Leyraud, A. Asamitsu, and L. Taillefer, Superconductivity in the noncentrosymmetric half-Heusler compound LuPtBi: A candidate for topological superconductivity, *Phys. Rev. B* **87**, 184504 (2013).
- [87] S. Groves and W. Paul, Band structure of gray tin, *Phys. Rev. Lett.* **11**, 194 (1963).
- [88] J. R. Chamorro, J. L. Zuo, E. N. Bassey, A. K. Watkins, G. Zhu, A. Zohar, K. E. Wyckoff, T. L. Kinnibrugh, S. H. Lapidus, S. Stemmer, R. J. Clément, S. D. Wilson, and R. Seshadri, Soft-chemical synthesis, structure evolution, and insulator-to-metal transition in pyrochlore-like λ - RhO_2 , *Chemistry of Materials* **36**, 1547 (2024).
- [89] I. Mandal, Search for plasmons in isotropic Luttinger semimetals, *Annals of Physics* **406**, 173 (2019).
- [90] I. Mandal, Tunneling in Fermi systems with quadratic band crossing points, *Annals of Physics* **419**, 168235 (2020).
- [91] S. Bera and I. Mandal, Floquet scattering of quadratic band-touching semimetals through a time-periodic potential well, *J. Phys. Condens. Matter* **33**, 295502 (2021).
- [92] S. Tchoumakov and W. Witczak-Krempa, Dielectric and electronic properties of three-dimensional Luttinger semimetals with a quadratic band touching, *Phys. Rev. B* **100**, 075104 (2019).
- [93] J. Wang and I. Mandal, Anatomy of plasmons in generic Luttinger semimetals, *Eur. Phys. J. B* **96**, 132 (2023).
- [94] M. P. Kennett, N. Komeilizadeh, K. Kaveh, and P. M. Smith, Birefringent breakup of Dirac fermions on a square optical lattice, *Phys. Rev. A* **83**, 053636 (2011).
- [95] B. Roy, P. M. Smith, and M. P. Kennett, Asymmetric spatial structure of zero modes for birefringent Dirac fermions, *Phys. Rev. B* **85**, 235119 (2012).
- [96] N. Komeilizadeh and M. P. Kennett, Instabilities of a birefringent semimetal, *Phys. Rev. B* **90**, 045131 (2014).
- [97] B. Dóra, J. Kailasvuori, and R. Moessner, Lattice generalization of the Dirac equation to general spin and the role of the flat band, *Phys. Rev. B* **84**, 195422 (2011).
- [98] H. Watanabe, Y. Hatsugai, and H. Aoki, Manipulation of the Dirac cones and the anomaly in the graphene related quantum Hall effect, *Journal of Physics: Conference Series* **334**, 012044 (2011).
- [99] Z. Lan, N. Goldman, A. Bermudez, W. Lu, and P. Öhberg, Dirac-Weyl fermions with arbitrary spin in two-dimensional optical superlattices, *Phys. Rev. B* **84**, 165115 (2011).
- [100] Z. Lan, A. Celi, W. Lu, P. Öhberg, and M. Lewenstein, Tunable multiple layered Dirac cones in optical lattices, *Phys. Rev. Lett.* **107**, 253001 (2011).
- [101] B. Bradlyn, J. Cano, Z. Wang, M. G. Vergniory, C. Felser, R. J. Cava, and B. A. Bernevig, Beyond Dirac and Weyl fermions: Unconventional quasiparticles in conventional crystals, *Science* **353**, aaf5037 (2016).
- [102] M. Ezawa, Pseudospin- $\frac{3}{2}$ fermions, type-II Weyl semimetals, and critical Weyl semimetals in tricolor cubic lattices, *Phys. Rev. B* **94**, 195205 (2016).
- [103] T. H. Hsieh, J. Liu, and L. Fu, Topological crystalline insulators and Dirac octets in antiperovskites, *Phys. Rev. B* **90**, 081112 (2014).
- [104] C. Chen, S.-S. Wang, L. Liu, Z.-M. Yu, X.-L. Sheng, Z. Chen, and S. A. Yang, Ternary wurtzite CaAgBi materials family: A playground for essential and accidental, type-I and type-II Dirac fermions, *Phys. Rev. Materials* **1**, 044201 (2017).
- [105] I. Mandal and H. Freire, Transport in the non-Fermi liquid phase of isotropic Luttinger semimetals, *Phys. Rev. B* **103**, 195116 (2021).
- [106] H. Freire and I. Mandal, Thermoelectric and thermal properties of the weakly disordered non-Fermi liquid phase of Luttinger semimetals, *Physics Letters A* **407**, 127470 (2021).

- [107] I. Mandal and H. Freire, Raman response and shear viscosity in the non-Fermi liquid phase of Luttinger semimetals, *Journal of Physics: Condensed Matter* **34**, 275604 (2022).
- [108] P. Dumitrescu, *Strongly Correlated Electron Systems Near Criticality: From Nodal Semimetals to High-Temperature Superconductors*, Ph.D. thesis, UC Berkeley (2016).
- [109] S. Sachdev, *Quantum Phase Transitions*, 2nd ed. (Cambridge University Press, 2011).
- [110] J. M. Luttinger, Theory of thermal transport coefficients, *Phys. Rev.* **135**, A1505 (1964).
- [111] J. Schmalian, *Lecture notes: Theory of condensed matter II* (2018).
- [112] H. Bruus and K. Flensberg, *Many-Body Quantum Theory in Condensed Matter Physics: An Introduction*, Oxford Graduate Texts (OUP Oxford, 2004).
- [113] L. P. Kadanoff and P. C. Martin, Hydrodynamic equations and correlation functions, *Annals of Physics* **24**, 419 (1963).
- [114] A. Rosch and N. Andrei, Conductivity of a clean one-dimensional wire, *Phys. Rev. Lett.* **85**, 1092 (2000).
- [115] E. Shimshoni, N. Andrei, and A. Rosch, Thermal conductivity of spin- $\frac{1}{2}$ chains, *Phys. Rev. B* **68**, 104401 (2003).
- [116] H. Freire, Controlled calculation of the thermal conductivity for a spinon Fermi surface coupled to a U(1) gauge field, *Ann. Phys. (N. Y.)* **349**, 357 (2014).
- [117] S. A. Hartnoll, R. Mahajan, M. Punk, and S. Sachdev, Transport near the Ising-nematic quantum critical point of metals in two dimensions, *Phys. Rev. B* **89**, 155130 (2014).
- [118] H. Freire, Memory matrix theory of the dc resistivity of a disordered antiferromagnetic metal with an effective composite operator, *Annals of Physics* **384**, 142 (2017).
- [119] H. Freire, Calculation of the magnetotransport for a spin-density-wave quantum critical theory in the presence of weak disorder, *Europhysics Letters* **118**, 57003 (2017).
- [120] H. Freire, Thermal and thermoelectric transport coefficients for a two-dimensional SDW metal with weak disorder: A memory matrix calculation, *EPL (Europhysics Letters)* **124**, 27003 (2018).
- [121] X. Wang and E. Berg, Scattering mechanisms and electrical transport near an Ising nematic quantum critical point, *Phys. Rev. B* **99**, 235136 (2019).
- [122] X. Wang and E. Berg, Low-frequency raman response near the ising-nematic quantum critical point: A memory-matrix approach, *Phys. Rev. B* **105**, 045137 (2022).
- [123] P. K. Kovtun, D. T. Son, and A. O. Starinets, Viscosity in strongly interacting quantum field theories from black hole physics, *Phys. Rev. Lett.* **94**, 111601 (2005).
- [124] S. A. Hartnoll and C. P. Herzog, Impure AdS/CFT correspondence, *Phys. Rev. D* **77**, 106009 (2008).
- [125] R. A. Davison, S. A. Gentle, and B. Goutéraux, Slow relaxation and diffusion in holographic quantum critical phases, *Phys. Rev. Lett.* **123**, 141601 (2019).
- [126] M. Blake, Universal charge diffusion and the butterfly effect in holographic theories, *Phys. Rev. Lett.* **117**, 091601 (2016).
- [127] M. Blake, Universal diffusion in incoherent black holes, *Phys. Rev. D* **94**, 086014 (2016).
- [128] J. Rau and B. Müller, From reversible quantum microdynamics to irreversible quantum transport, *Physics Reports* **272**, 1 (1996).
- [129] S. A. Hartnoll and D. M. Hofman, Locally critical resistivities from Umklapp scattering, *Phys. Rev. Lett.* **108**, 241601 (2012).
- [130] R. A. Davison, B. Goutéraux, and S. A. Hartnoll, Incoherent transport in clean quantum critical metals, *Journal of High Energy Physics* **2015**, 112 (2015).
- [131] S. A. Hartnoll, P. K. Kovtun, M. Müller, and S. Sachdev, Theory of the Nernst effect near quantum phase transitions in condensed matter and in dyonic black holes, *Phys. Rev. B* **76**, 144502 (2007).
- [132] P. Giraldo-Gallo, J. A. Galvis, Z. Stegen, K. A. Modic, F. F. Balakirev, J. B. Betts, X. Lian, C. Moir, S. C. Riggs, J. Wu, A. T. Bollinger, X. He, I. Božović, B. J. Ramshaw, R. D. McDonald, G. S. Boebinger, and A. Shekhter, Scale-invariant magnetoresistance in a cuprate superconductor, *Science* **361**, 479 (2018).
- [133] M. P. A. Fisher, P. B. Weichman, G. Grinstein, and D. S. Fisher, Boson localization and the superfluid-insulator transition, *Phys. Rev. B* **40**, 546 (1989).
- [134] L. Huijse, S. Sachdev, and B. Swingle, Hidden fermi surfaces in compressible states of gauge-gravity duality, *Phys. Rev. B* **85**, 035121 (2012).
- [135] J. M. Luttinger, Quantum theory of cyclotron resonance in semiconductors: General theory, *Phys. Rev.* **102**, 1030 (1956).
- [136] L. Janssen and I. F. Herbut, Nematic quantum criticality in three-dimensional fermi system with quadratic band touching, *Phys. Rev. B* **92**, 045117 (2015).
- [137] I. Boettcher and I. F. Herbut, Superconducting quantum criticality in three-dimensional Luttinger semimetals, *Phys. Rev. B* **93**, 205138 (2016).
- [138] B. Roy, S. A. A. Ghorashi, M. S. Foster, and A. H. Nevidomskyy, Topological superconductivity of spin-3/2 carriers in a three-dimensional doped Luttinger semimetal, *Phys. Rev. B* **99**, 054505 (2019).
- [139] J. M. Link and I. F. Herbut, Hydrodynamic transport in the Luttinger-Abrikosov-Beneslavskii non-Fermi liquid, *Phys. Rev. B* **101**, 125128 (2020).
- [140] A. Mauri and M. Polini, Dielectric function and plasmons of doped three-dimensional Luttinger semimetals, *Phys. Rev. B* **100**, 165115 (2019).
- [141] I. Boettcher, Optical response of Luttinger semimetals in the normal and superconducting states, *Phys. Rev. B* **99**, 125146 (2019).
- [142] S. Bera and I. Mandal, Floquet scattering of quadratic band-touching semimetals through a time-periodic potential well, *Journal of Physics: Condensed Matter* **33**, 295502 (2021).
- [143] S. Murakami, N. Nagosa, and S.-C. Zhang, SU(2) non-abelian holonomy and dissipationless spin current in semiconductors, *Phys. Rev. B* **69**, 235206 (2004).
- [144] I. F. Herbut, Isospin of topological defects in Dirac systems, *Phys. Rev. B* **85**, 085304 (2012).
- [145] K. G. Wilson and M. E. Fisher, Critical exponents in 3.99 dimensions, *Phys. Rev. Lett.* **28**, 240 (1972).
- [146] M. E. Peskin and D. V. Schroeder, *An Introduction to Quantum Field Theory* (Addison-Wesley, Reading, 1995).
- [147] A. Schliefl, P. Lunts, and S.-S. Lee, Exact critical exponents for the antiferromagnetic quantum critical metal in two dimensions, *Phys. Rev. X* **7**, 021010 (2017).
- [148] H. Kumar, K. C. Kharkwal, K. Kumar, K. Asokan, A. Banerjee, and A. K. Pramanik, Magnetic and transport properties of the pyrochlore iridates $(Y_{1-x}Pr_x)_2Ir_2O_7$: Role of $f-d$ exchange interaction and $d-p$ orbital hybridization, *Phys. Rev. B* **101**, 064405 (2020).
- [149] I. Bozovic, D. Kirillov, A. Kapitulnik, K. Char, M. R. Hahn, M. R. Beasley, T. H. Geballe, Y. H. Kim, and A. J. Heeger, Optical measurements on oriented thin $yba_2cu_3o_{7-\delta}$ films: Lack of evidence for excitonic superconductivity, *Phys. Rev. Lett.* **59**, 2219 (1987).
- [150] S. L. Cooper, F. Slakey, M. V. Klein, J. P. Rice, E. D. Bukowski, and D. M. Ginsberg, Gap anisotropy and phonon self-energy effects in single-crystal $YBa_2Cu_3O_{7-\delta}$,

- Phys. Rev. B* **38**, 11934 (1988).
- [151] T. Stauffer, R. Hackl, and P. Müller, Some new aspects of the electronic response in Cu-O superconductors, *Solid State Communications* **79**, 409 (1991).
- [152] F. Slakey, M. V. Klein, J. P. Rice, and D. M. Ginsberg, Raman investigation of the $\text{YBa}_2\text{Cu}_3\text{O}_7$ imaginary response function, *Phys. Rev. B* **43**, 3764 (1991).
- [153] T. P. Devereaux and R. Hackl, Inelastic light scattering from correlated electrons, *Reviews of Modern Physics* **79**, 175 (2007).
- [154] C. Cao, E. Elliott, J. Joseph, H. Wu, J. Petricka, T. Schäfer, and J. E. Thomas, Universal quantum viscosity in a unitary Fermi gas, *Science* **331**, 58 (2011).
- [155] L. Fritz, J. Schmalian, M. Müller, and S. Sachdev, Quantum critical transport in clean graphene, *Phys. Rev. B* **78**, 085416 (2008).
- [156] E. Taylor and M. Randeria, Viscosity of strongly interacting quantum fluids: Spectral functions and sum rules, *Phys. Rev. A* **81**, 053610 (2010).
- [157] T. Enss, R. Haussmann, and W. Zwerger, Viscosity and scale invariance in the unitary fermi gas, *Annals of Physics* **326**, 770 (2011).
- [158] P. T. Dumitrescu, Shear viscosity in a non-Fermi-liquid phase of a quadratic semimetal, *Phys. Rev. B* **92**, 121102 (2015).
- [159] M. Rosalin, P. Telang, S. Singh, D. V. S. Muthu, and A. K. Sood, Non-Fermi-liquid signatures of quadratic band touching and phonon anomalies in metallic $\text{Pr}_2\text{Ir}_2\text{O}_7$, *Phys. Rev. B* **108**, 195144 (2023).
- [160] Shama, R. Gopal, and Y. Singh, Observation of planar Hall effect in the ferromagnetic Weyl semimetal $\text{Co}_3\text{Sn}_2\text{S}_2$, *Journal of Magnetism and Magnetic Materials* **502**, 166547 (2020).
- [161] P. Li, C. H. Zhang, J. W. Zhang, Y. Wen, and X. X. Zhang, Giant planar Hall effect in the Dirac semimetal ZrTe_5 , *Phys. Rev. B* **98**, 121108 (2018).
- [162] A. Roy Karmakar, S. Nandy, A. Taraphder, and G. P. Das, Giant anomalous thermal Hall effect in tilted type-I magnetic Weyl semimetal $\text{Co}_3\text{Sn}_2\text{S}_2$, *Phys. Rev. B* **106**, 245133 (2022).
- [163] R. Ghosh and I. Mandal, Electric and thermoelectric response for Weyl and multi-Weyl semimetals in planar Hall configurations including the effects of strain, *Physica E: Low-dimensional Systems and Nanostructures* **159**, 115914 (2024).
- [164] S. Yadav, S. Fazzini, and I. Mandal, Magneto-transport signatures in periodically-driven Weyl and multi-Weyl semimetals, *Physica E Low-Dimensional Systems and Nanostructures* **144**, 115444 (2022).
- [165] K. Behnia, M.-A. Méasson, and Y. Kopelevich, Nernst effect in semimetals: The effective mass and the figure of merit, *Phys. Rev. Lett.* **98**, 076603 (2007).
- [166] I. Mandal and K. Saha, Thermopower in an anisotropic two-dimensional Weyl semimetal, *Physical Review B* **101** (2020).
- [167] M. Papaj and L. Fu, Magnus Hall effect, *Phys. Rev. Lett.* **123**, 216802 (2019).
- [168] D. Mandal, K. Das, and A. Agarwal, Magnus Nernst and thermal Hall effect, *Phys. Rev. B* **102**, 205414 (2020).
- [169] Sekh, Sajid and Mandal, Ipsita, Magnus Hall effect in three-dimensional topological semimetals, *Eur. Phys. J. Plus* **137**, 736 (2022).
- [170] D. Stanford, Many-body chaos at weak coupling, *Journal of High Energy Physics* **2016** (2016).
- [171] M. Blake, Universal charge diffusion and the butterfly effect in holographic theories, *Phys. Rev. Lett.* **117**, 091601 (2016).
- [172] M. Blake, Universal diffusion in incoherent black holes, *Phys. Rev. D* **94**, 086014 (2016).
- [173] J. Maldacena, S. H. Shenker, and D. Stanford, A bound on chaos, *Journal of High Energy Physics* **2016** (2016).
- [174] J. Maldacena and D. Stanford, Remarks on the Sachdev-Ye-Kitaev model, *Physical Review D* **94** (2016).
- [175] S. H. Shenker and D. Stanford, Black holes and the butterfly effect, *Journal of High Energy Physics* **2014** (2014).
- [176] B. Cheng, T. Ohtsuki, D. Chaudhuri, S. Nakatsuji, M. Lippmaa, and N. P. Armitage, Dielectric anomalies and interactions in the three-dimensional quadratic band touching Luttinger semimetal $\text{Pr}_2\text{Ir}_2\text{O}_7$, *Nature Communications* **8**, 2097 (2017).
- [177] Z. Tian, Y. Kohama, T. Tomita, H. Ishizuka, T. H. Hsieh, J. J. Ishikawa, K. Kindo, L. Balents, and S. Nakatsuji, Field-induced quantum metal-insulator transition in the pyrochlore iridate $\text{Nd}_2\text{Ir}_2\text{O}_7$, *Nature Physics* **12**, 134 (2016).
- [178] A. Damascelli, Z. Hussain, and Z.-X. Shen, Angle-resolved photoemission studies of the cuprate superconductors, *Rev. Mod. Phys.* **75**, 473 (2003).
- [179] M. Mitrano, A. A. Husain, S. Vig, A. Kogar, M. S. Rak, S. I. Rubeck, J. Schmalian, B. Uchoa, J. Schneeloch, R. Zhong, G. D. Gu, and P. Abbamonte, Anomalous density fluctuations in a strange metal, *Proceedings of the National Academy of Sciences* **115**, 5392 (2018).
- [180] A. A. Husain, M. Mitrano, M. S. Rak, S. Rubeck, B. Uchoa, K. March, C. Dwyer, J. Schneeloch, R. Zhong, G. D. Gu, and P. Abbamonte, Crossover of charge fluctuations across the strange metal phase diagram, *Phys. Rev. X* **9**, 041062 (2019).
- [181] A. A. Husain, E. W. Huang, M. Mitrano, M. S. Rak, S. I. Rubeck, X. Guo, H. Yang, C. Sow, Y. Maeno, B. Uchoa, T. C. Chiang, P. E. Batson, P. W. Phillips, and P. Abbamonte, Pines' demon observed as a 3D acoustic plasmon in Sr_2RuO_4 , *Nature* **621**, 66 (2023).